AN OPERATIONAL TECHNIQUE FOR ESTIMATING VISIBLE SPECTRUM CONTRAST TRANSMITTANCE

Wayne S. Hering

Visibility Laboratory
University of California, San Diego
Scripps Institution of Oceanography
La Jolla, California 92093

Approved:

Roswell W. Austin, Director
Visibility Laboratory

Approved:

William A. Nierenberg, Director
Scripps Institution of Oceanography

CONTRACT NO. F19628-78-C-0200
Project No. 7670
Task No. 7670-14
Work Unit No. 7670-14-01

Scientific Report No. 16
June 1981

Contract Monitor
Major John D. Mill, Atmospheric Optics Branch, Optical Physics Division

Prepared for

AIR FORCE GEOPHYSICS LABORATORY
AIR FORCE SYSTEMS COMMAND
UNITED STATES AIR FORCE
HANSCOM AFB, MASSACHUSETTS 01731

SUMMARY

Simultaneous optical and meteorological measurements between ground level and 6 km altitude gathered by the Visibility Laboratory in recent years in the United States and Europe with an instrumented aircraft have provided the basis for the development of a technique for estimating atmospheric path radiance and directional contrast transmittance. The technique is relatively fast and easy to apply yet is designed to take full advantage of the present limited capability to observe and predict the relevant atmospheric variables. Various modelling approximations are introduced to simplify the calculations of radiative transfer and to help specify the vertical distribution of atmospheric attenuation coefficient and the single scattering phase function. Critical examinations of the assumptions and approximations were made through reference to the extensive series of airborne meteorological/optical measurements. Model input parameters are the number of atmospheric layers selected and the average optical scattering ratio and single scattering albedo for each layer, the solar zenith angle, the extra-terrestrial solar irradiance, a representative wavelength and the surface reflectance. The computer program calculates the sky and terrain radiance corresponding to any selected point and direction and the contrast transmittance for any slant atmospheric path.

The changes in image transmittance characteristics that are associated with the natural variations in environmental physical parameters are examined through systematic application of the modelling techniques. Comparisons are made of the calculated changes in visible spectrum contrast transmittance that result from typical changes in the optical thickness of the low-level haze layer, the aerosol absorption, the surface spectral reflectance, the solar zenith angle and the viewing path.

TABLE OF CONTENTS

SUMMARY v

1. INTRODUCTION 1

2. THEORETICAL DEVELOPMENT AND COMPARISONS WITH OTHER MODEL RESULTS 1

   2.1 Calculation of Path Function 2
   2.2 Calculation of Sky and Terrain Radiance 3
   2.3 Comparisons with Other Model Calculations 3

3. SPECIFICATION OF THE VERTICAL DISTRIBUTION OF TOTAL VOLUME SCATTERING COEFFICIENT 6

   3.1 Scattering Ratio Specification 6
   3.2 Specification of Haze Layer Depth 7
   3.3 Summary of Proposed Technique for the Specification of the Scattering Coefficient Profile in the Troposphere 8

4. SINGLE SCATTERING PHASE FUNCTION REPRESENTATION 9

5. COMPUTER APPLICATION OF MODELLING TECHNIQUES 11

   5.1 Model Results and Comparisons with Measured Data 11

6. SENSITIVITY OF SPECTRAL CONTRAST TRANSMITTANCE TO SELECTED CHANGES IN PHYSICAL PARAMETERS 16

   6.1 Object at the Earth's Surface and the Sensor at 6 km 16
   6.2 Object at 6 km and the Sensor at Ground Level 16
   6.3 Object at the Surface and Sensor at 20 km 19

7. SUMMARY COMMENTS 19

8. ACKNOWLEDGEMENTS 20

9. REFERENCES 20

APPENDIX A: DERIVATION OF THE COMPONENT OF PATH RADIANCE DUE TO THE DIRECTIONAL SCATTERING OF DIFFUSE RADIANCE USING THE DELTA EDDINGTON APPROXIMATION 21

APPENDIX B: SUMMARY OF INPUT DATA, COMPUTATION STEPS, AND RESULTANT OUTPUT FOR CONTRAST TRANSMITTANCE MODEL 22

APPENDIX C: SPECIFIC INPUT DATA FOR MODEL CALCULATIONS 23

APPENDIX D: GLOSSARY AND NOTATION 24

LIST OF ILLUSTRATIONS

Fig. No.		Page
2-1	Comparison of radiance calculations with other model results for haze cases	4
2-2	Comparison of radiance calculations with other model results for cloud case with no absorption	5
2-3	Comparison of radiance calculations with other model results for cloud case with absorption	5
3-1	Model representation of scattering coefficient profiles	7
3-2	Simultaneous profiles of scattering ratio, lapse rate and temperature	8
4-1	Model calculations of single scattering phase functions for haze case	10
4-2	Model calculations of single scattering phase functions for cloud case	10
5-1	Comparison between measured and calculated radiance for flight C-466 at altitude 203m	12
5-2	Comparison between measured and calculated radiance for flight C-466 at altitude 6000m	12
5-3	Comparison between measured and calculated radiance for flight C-401 at altitude 996m	13
5-4	Comparison between measured and calculated radiance for flight C-401 at altitude 5290m	13
5-5	Comparison between measured and calculated radiance for flight C-469, blue filter, at altitude 277m	14
5-6	Comparison between measured and calculated radiance for flight C-469, blue filter, at altitude 5838m	14
5-7	Comparison between measured and calculated radiance for flight C-469, near infrared filter, at altitude 280m	15
5-8	Comparison between measured and calculated radiance for flight C-469, near infrared filter at altitude 5880m	15
6-1	Diagnostic calculations of contrast transmittance for downward path of sight	17
6-2	Variations in target acquisition range for downward path of sight associated with changes in: (a) optical thickness, (b) solar zenith angle, (c) surface reflectance and (d) absorption	17
6-3	Diagnostic calculations of contrast transmittance for upward paths of sight	18
6-4	Variations in target acquisition range for upward path of sight with changes in: (a) optical thickness, (b) solar zenith angle, (c) surface reflectance and (d) absorption	18
6-5	Effects of parametric environmental changes on contrast transmittance	19

AN OPERATIONAL TECHNIQUE FOR ESTIMATING VISIBLE SPECTRUM CONTRAST TRANSMITTANCE

1. INTRODUCTION

The visual detection of distant objects is restricted by air molecule and aerosol particle scattering and to a lesser extent by atmospheric absorption. The complexity of multiple scattering and absorption processes and the inherent variability of the aerosol particle distribution and composition require effective simplifications in order that estimates of contrast transmittance through the atmosphere can be made rapidly and consistently.

A series of modelling approximations that relate optical scattering properties to meteorological variables are derived from experimental data and combined with available analytic approximations for radiative transfer calculations to develop an operational technique for the estimation of directional path radiance and directional slant-path contrast transmittance. The approach involves validation of the individual elements of the procedure through reference to simultaneous optical and meteorological measurements gathered by the Visibility Laboratory (Johnson *et al.*, 1979) over the past several years with a specially instrumented Air Force C-130 aircraft under sponsorship of the Air Force Geophysics Laboratory. The high resolution profile measurements were made in a wide range of meteorological and geographical conditions in the United States and western Europe.

The path contrast transmittance in the visible spectrum depends most critically upon the distribution of total volume scattering coefficient, both along the path and in the surrounding atmosphere. Accordingly, an attempt was made to condition the approximation procedures for the radiative transfer calculations and for all input parameters in a manner consistent with the existing capability to model and predict the scattering coefficient structure and behavior.

2. THEORETICAL DEVELOPMENT AND COMPARISONS WITH OTHER MODEL RESULTS

Neglecting turbulence effects, the equation for the apparent spectral radiance of the background b at range r along the path of sight specified by zenith angle θ and azimuthal angle ϕ, can be written (Duntley *et al.*, 1957)

$$ {}_bL_r(z,\theta,\phi) = T_r(z,\theta)\,{}_bL_o(z_t,\theta,\phi) + L_r^*(z,\theta,\phi)\,, \qquad (1) $$

where ${}_bL_o$ is the inherent background radiance at target altitude z_t, $T_r = \exp -\int_o^r \alpha(r)\,dr$ is the path transmittance, α is the volume attenuation coefficient, and L_r^* is the path radiance produced by the scattering of light from the sun and from the surrounding sky and terrain into the path of sight.

The path radiance is given by

$$ L_r^*(z,\theta,\phi) = \int_o^r L_*(z',\theta,\phi)\,T_r(z',\theta)\,dr'\,, \qquad (2) $$

where $L_*(z',\theta,\phi)$ is the path function, defined as the point function component of path radiance generated by the directional scattering of light reaching that point of the path. The expression for the path function can be written in terms of its contributions from the scattering of solar scalar irradiance ${}_s\epsilon(z)$ and from the scattering of sky and earth radiances $L(z,\theta',\phi')$ as follows (Gordon, 1969):

$$ L_*(z,\theta,\phi) = {}_s\epsilon(z)\sigma(z,\beta_s) + \int_{4\pi} L(z,\theta',\phi')\sigma(z,\beta')\,d\Omega'\,, \qquad (3) $$

where $\sigma(z,\beta)$ is the directional volume scattering function at angle β between the path of sight and direction of the source light, $d\Omega$ is an element of solid angle, and β_s is the scattering angle with respect to the sun.

In turn, the spectral contrast transmittance of the path of sight can be expressed (see Duntley *et al.*, 1957) directly as the product of the path transmittance, $T_r(z,\theta)$, and the ratio of the inherent, ${}_bL_o$, and apparent, ${}_bL_r$, background radiances as follows:

$$ C_r(z,\theta,\phi)/C_o(z_t,\theta,\phi) = T_r(z,\theta)\,{}_bL_o(z_t,\theta,\phi)/{}_bL_r(z,\theta,\phi)\,, \qquad (4) $$

where $C_r = ({}_tL_r - {}_bL_r)/{}_bL_r$ is the apparent target contrast at path length r, $C_o = ({}_tL_o - {}_bL_o)/{}_bL_o$ is the inherent target contrast at altitude z_t and ${}_tL_o$ is the inherent target radiance. Thus, the contrast transmittance of a given path does not depend upon intrinsic target characteristics but is a function only of the directional radiance distribution in the atmosphere and the path transmittance. The expres-

sion is strictly applicable only for monochromatic radiation but may be applied with good approximation to reasonably broad spectral bands in the visible portion of the spectrum.

From Eq. (3) we note that the path function and in turn the contrast transmittance as calculated from Eq. (4) depend upon the direction of the viewing path relative to the distribution of light reaching the path. The first term on the right hand side of Eq. (3) is the contribution of primary scattering of direct solar irradiance. The directional volume scattering function may be expressed

$$\sigma(z,\beta) = P(z,\beta)s(z)\,, \tag{5}$$

where $s(z)$ is the total volume scattering coefficient, and $P(z,\beta)$ is the single scattering phase function, which defines the probability that incident radiation will be scattered in the direction given by scattering angle β. The phase function varies significantly with the scattering properties of the aerosol particle distribution in the atmosphere. Modelling procedures used herein either accept $P(z,\beta)$ as calculated from theory from an assumed or measured particle size distribution or use an analytic representation of $P(z,\beta)$ as described in Section 4 of this paper.

Substituting Eq. (5) in Eq. (3), the expression for $L_*(z,\theta,\phi)$ becomes

$$L_*(z,\theta,\phi) = {}_s\epsilon(z)P(z,\beta)s(z) + \int\int_{4\pi} L(z,\theta',\phi')P(z,\beta)s(z)d\Omega'\,. \tag{6}$$

Modelling techniques for the calculation of the diffuse component of the path function are discussed in the following paragraphs.

2.1 Calculation of the Path Function

The second term on the right hand side of Eq. (6) is the component of the path function resulting from the scattering of diffuse radiance reaching the path from the surrounding sky and terrain. It has a directional dependence due to the asymmetry in the sky and earth radiances illuminating the path and in the scattering phase function. Precise numerical calculation of the path radiance resulting from the complex multiple scattering processes requires large amounts of computer time. For this reason, rapid approximate methods are employed extensively for radiation transfer calculations. The appropriate choice of computational method from among the variety of available methods depends upon the results desired for the application at hand.

While it is important to retain complete directionality for calculation of the path radiance component due to single scattering of direct solar radiance, approximate hemispherical two stream methods can be used effectively for fast calculation of the path radiance component due to scattering of the background sky and terrain radiances at any point and direction provided that the asymmetric influence of the prominent forward scatter peak and the irradiance profile are managed adequately. The delta-Eddington approximation introduced by Joseph, Wiscombe and Weinman (1976) satisfies the requirement. It differs from the standard Eddington approximation, which assumes a simple cosine dependence of the single scattering phase function, in that it approximates the phase function by a truncated forward scatter peak and a two-term phase function expansion,

$$4\pi P_d(\beta) = 2f'\,\delta(1-\cos\beta) + (1-f')(1+3g'\cos\beta) \tag{7}$$

where f' is the fractional scattering represented by the forward peak and g' is the asymmetry factor of the truncated phase function. In effect, the delta-Eddington approximation transforms most of the enhanced radiance in the solar aureole into the direct solar flux component, and assumes

$$f'(z) = g^2(z)\,. \tag{8}$$

Joseph *et al.*, (1976) show that calculations of radiative transfer with the delta-Eddington approximation can be carried out with the standard Eddington computer code (Shettle and Weinman, 1970) with the following changes of variable

$$\Delta\tau' = (1-\omega f')\,\Delta\tau\,, \tag{9}$$

$$\omega' = \omega(1-f')/(1-\omega f')\,, \tag{10}$$

and

$$g' = (g-f')/(1-f')\,, \tag{11}$$

where $\Delta\tau$ is the optical thickness of the layer and ω is the single scattering albedo.

As an integral part of the technique for estimating directional contrast transmittance, the products of the Eddington computer code (Shettle and Weinman, 1970) are used directly to calculate the second term on the right hand side of Eq. (6).

From the standard Eddington approximation, the diffuse radiance is assumed to be given by

$$L(z,\theta',\phi') = L_D(z) + L_{D'}(z)\cos\theta'\,. \tag{12}$$

In accordance with the derivation given in Appendix A, if we substitute Eq. (12) and the delta-Eddington approximations given by Eq. (7), (8) and (11) into the last term of Eq. (6) and integrate over θ' and ϕ', we have

$$\int\int_{4\pi} L(z,\theta',\phi')P(z,\beta)s(z)d\Omega \qquad (13)$$

$$= s(z)\,[L_D(z) + gL_{D'}(z)\cos\theta]\,.$$

Commensurate with the delta-Eddington approximations and Eq. (9), the expression for the solar scalar irradiance at altitude z is

$${}_s\epsilon(z) = {}_s\epsilon(\infty)\exp(-\tau'/\cos\theta_s)\,, \qquad (14)$$

where ${}_s\epsilon(\infty)$ is the extraterrestrial solar scalar irradiance.

Substituting Eqs. (13) and (14) into Eq. (6), the expression for the path function becomes

$$L_*(z,\theta,\phi) = s(z)\,[\,P(z,\beta_s)\,{}_s\epsilon(\infty)\exp(-\tau'/\cos\theta_s) \qquad (15)$$
$$+ L_D + gL_D\cos\theta\,]\,.$$

2.2 Calculation of Sky and Terrain Radiance

For an assumed plane parallel and horizontally homogeneous atmosphere, the directional path radiance, $L_r^*(z,\theta,\phi)$, and the radiance, $L(z,\theta,\phi)$, can now be calculated from Eqs. (1), (2) and (15) through finite summation over adjacent atmospheric layers using the trapezoidal rule. For upward paths of sight the inherent background radiance at target altitude is given by

$${}_bL_o(z_t,\theta,\phi) = L_\infty^*(z_t,\theta,\phi)\,, \qquad (16)$$

where $L_\infty^*(z_t,\theta,\phi)$ is the path radiance as determined at altitude z_t for the path of sight from the top of the atmosphere to z_t. Looking downward, the inherent background radiance is given by

$${}_bL_o(z_t,\theta,\phi) = T_{ro}(z_t,\theta)R(\theta,\phi)E(0,d)/\pi \qquad (17)$$
$$+ L_{ro}^*(z_t,\theta,\phi)\,,$$

where $R(\theta,\phi)$ is the directional surface reflectance, $E(0,d) = {}_sE(0)\cos\theta_s + \pi[L_D(0) + 2/3L_{D'}(0)\,]$ is the downwelling irradiance at the surface, and T_{ro} is the transmittance of the slant path from the surface to target altitude z_t.

2.3 Comparisons with Other Model Calculations

The extensive series of optical and meteorological measurements, referenced in Section 1, has been used to test individual modelling approximations and to help validate the integrated application of the techniques. For example, in Section 5 model calculations of sky and terrain radiance based upon the procedures set forth in Sections 2, 3 and 4, are compared with the high resolution measurements of the spectral radiance made with the instrumented aircraft.

Additional tests were carried out to evaluate specifically the approximations for the radiative transfer calculations as described above. Model calculations of radiance distributions were compared with the theoretical results as calculated from comprehensive radiative transfer models, which are mathematically precise but in general require relatively large computer capacity and time for the radiance calculations. For these tests, the comparative accuracy was determined under the assumption that the physical system is perfectly observed, and the input data are identical for the approximate operational model and the comprehensive numerical models. The set of examples selected for tests by the ad hoc Working Group of the Radiation Commission, International Association of Meteorology and Atmospheric Physics (Lenoble, 1977) were used for the analysis. The results of the spherical harmonic method listed in the Working Group report were chosen for a reference standard since comparative calculations using this method were presented for all five test cases. A single layer, plane parallel and homogeneous atmosphere with a black underlying surface was prescribed in each case. Three cases have a Haze L (Diermendjian, 1969) aerosol particle distribution with an optical thickness of 1, and the other two have assumed cloud particle distributions with an optical thickness of 64. The phase function for single scattering and the single scattering albedo are specified for each case. The comparative results of the radiance calculations as summarized over all listed interior verification levels (5) and zenith view angles (11) are given for each case (including a subset for each of 3 azimuthal angles for case 3) in Table 2.1, and some graphical comparisons of test results are shown in Figs. 2-1, 2-2, and 2-3.

It is important to note that the agreement among the more rigorous numerical methods, including the Monte Carlo techniques, as given in the Working Group report, was generally within a few percent depending upon the completeness of scattering history retained in the calculations. We see from Table 2.1 and Fig. 2-1 that the departures of the simplified model radiance calculations from the reference values for the haze cases are significantly larger, yet the indicated accuracy is good when considered in context with the uncertainties and completeness of the observational data base from which the estimates must be derived in operational practice. The simplified model requires only a few seconds of large scale computer time for each case, and the model is designed for easy microprocessor application for real time requirements. Except for the subset of case 3 with the azimuthal view angle directly upsun, $\phi = 0°$, the logarithmic rms error of specification for the haze cases was between 0.11 and 0.16 (or approximately 11 to 16 percent rms error). The approximations inherent in the operational model serve to smooth out the azimuthal asymmetry in the calculated radiance component due to the scattering of incident diffuse light; hence the increase in rms error for the subset $\phi = 0°$. It is expected that the error of estimate would continue to increase in the solar azimuthal plane in the forward scattering direction as the solar zenith angle increases beyond the assumed 60° for case 3.

Table 2.1.

Summary of numerical comparisons of radiance calculations by the operational model and by the spherical harmonics method as listed in the Working Group Report (Lenoble, 1977) of the Radiation Commission, IAMAP, for 5 reference atmospheres.

Case	Atmosphere	Optical Thickness	Single Scattering Albedo	Solar Zenith Angle	Percent (1) Reduction of Variance	Logarithmic rms Error (2)
1	Haze L	1	1.0	0°	98.6	.148
2	Haze L	1	0.9	0°	99.2	.114
3A	Haze L ($\phi = 0°$)	1	0.9	60°	96.8	.321
3B	Haze L ($\phi = 90°$)	1	0.9	60°	97.4	.153
3C	Haze L ($\phi = 180°$)	1	0.9	60°	97.4	.158
4	Cloud	64	1.0	0°	98.4*	.053*
5	Cloud	64	0.9	0°	99.4*	.304*

* As noted in the text, the calculated values for $L(\tau,0,0)$ are not included in the cloud case summaries.

(1) Percent reduction of variance is given by the square of correlation coefficient between $\ln L_{hi}$ (harmonic model) and $\ln L_{oi}$ (operational model)

(2) Logarithmic rms error = $\left[\sum_{i=1}^{N} (\ln L_{hi} - \ln L_{oi})^2/N\right]^{1/2}$

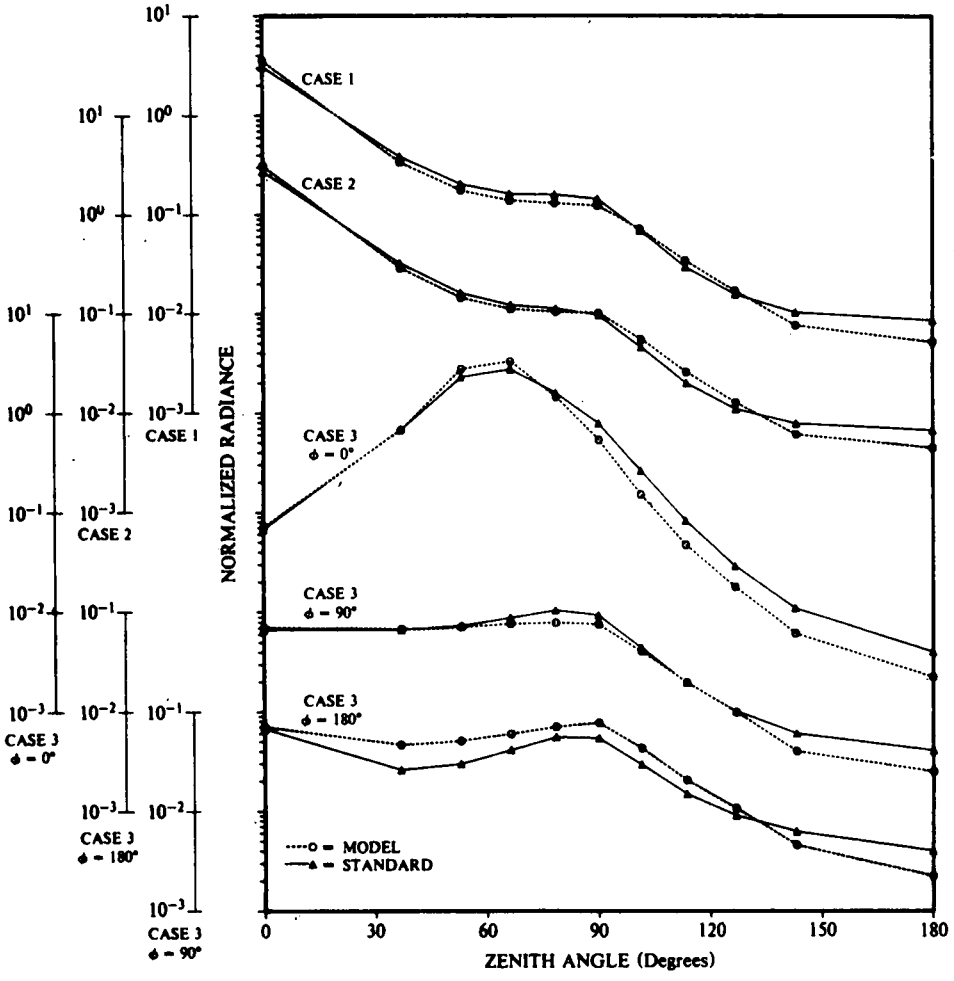

Fig. 2-1. Calculated radiance as a function of zenith angle for optical depth 0.75 for cases 1, 2, and 3 ($\phi = 0°$, 90°, 180°). Model results (dashed lines) are compared with the results computed with the spherical harmonics method (Lenoble, 1977) (solid lines). The results are for single layer atmospheres assuming the Haze L distribution of Diermendjian (1969) and with the solar zenith angle and single scattering albedo as given in Table 2.1. The incident solar flux is assumed equal to π.

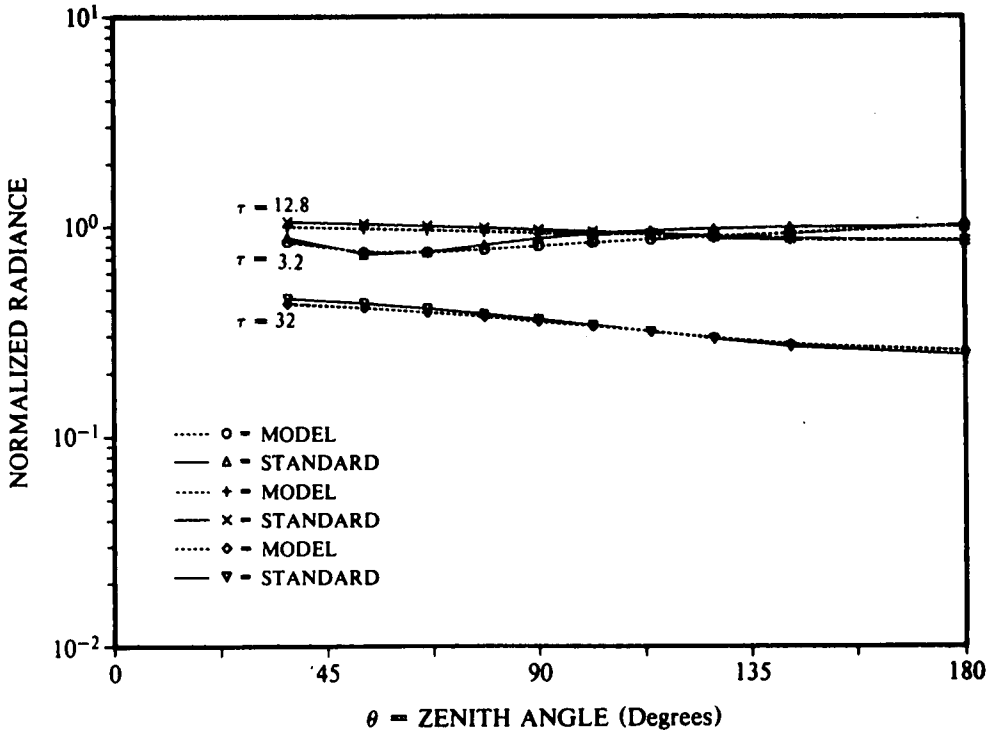

Fig. 2-2. Calculated radiance as a function of zenith angle for cloud case 4 at 3 interior levels with optical depths 3.2, 12.8 and 32. Model results (dashed lines) are compared with the computations by the spherical harmonics method (solid lines) for the cloud layer assuming no absorption and overhead sun.

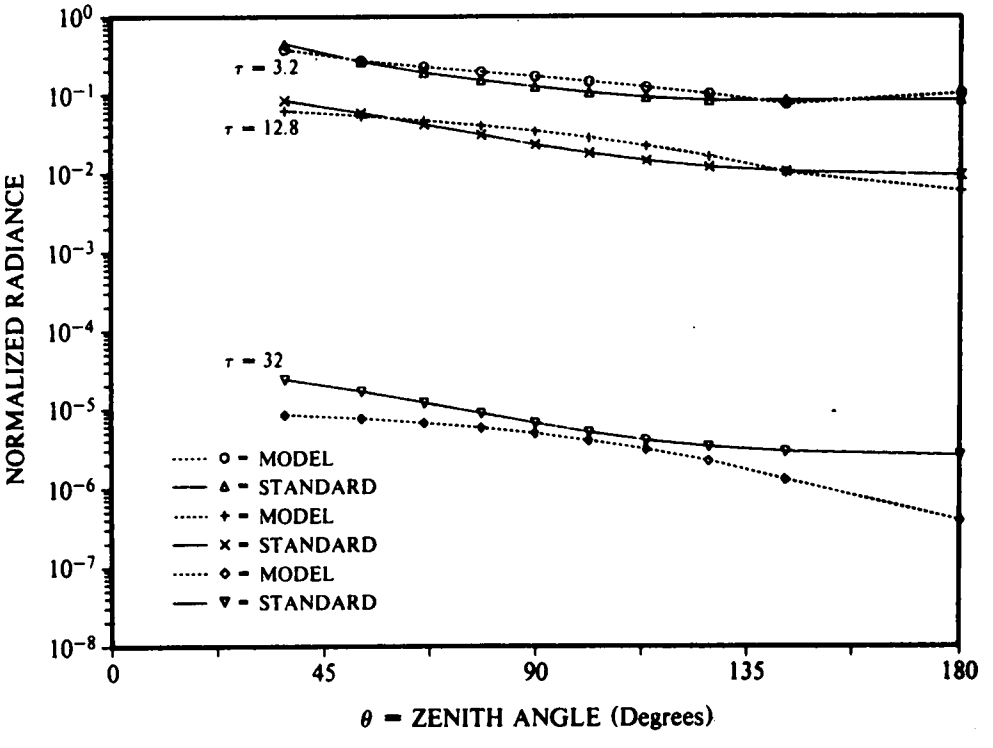

Fig. 2-3. Same as Fig. 2-2 except for case 5 with single scattering albedo of 0.9.

The results for the cloud cases listed in Table 2.1 and shown in Figs. 2-2 and 2-3 are based on the asymptotic solution to the model equations, where the radiance distribution at any point interior to the cloud is given simply by the equilibrium radiance, $L_q(z,\theta,\phi) = L_*(z,\theta,\phi)/\alpha(z)$. Although the technique was not developed for a cloud environment, it was found that the calculated equilibrium radiance represents the directional distributions of spectral radiance for the two reference cloud layers with an overhead sun with good accuracy. However, equilibrium radiance does not obtain for the viewing paths directly upsun and the asymptotic solution yields excessively large values of calculated radiance for $\theta = \theta_s = 0$. The predominant error anomalies for the directional radiance $L(\tau,0,0)$ are not included in the comparative statistics for the cloud cases, so that the summaries listed in Table 2.1 for cases 4 (no absorption) and 5 (with absorption) cover 10 zenith viewing angles extending from 37° to 180° and 5 optical thickness levels within the cloud. The calculated radiance reduces by several orders of magnitude at optical depth 32 for the absorption case (see Fig. 2-3) as compared with a much smaller decrease with increasing optical depth for the conservative case (Fig. 2-2). The equilibrium radiance solution provides reasonably good specification of absolute radiance at large optical depths for both cases but the percentage departure from the reference model calculations increases with increasing depth for the cloud case with absorption (Fig. 2-3).

3. SPECIFICATION OF THE VERTICAL DISTRIBUTION OF TOTAL VOLUME SCATTERING COEFFICIENT

The spatial distribution of total volume scattering coefficient is the major determinant of visible spectrum contrast transmittance. Techniques for the specification of the scattering coefficient profile have been investigated during the course of the aircraft measurement and analysis program (Johnson *et al.*, 1979). Some of the results of these studies and their application to operational modelling procedures are summarized in this section.

3.1 Scattering Ratio Specification

For profile modelling purposes, it is important to consider a conservative measure of scattering coefficient that in the absence of local aerosol particle sources or sinks does not change appreciably following the air motion. The optical scattering mixing ratio, $Q(z)$, is such a parameter. As the vertical mixing within an identifiable atmospheric layer becomes more complete, $Q(z)$ becomes more constant with height within the layer.

The optical scattering ratio is defined

$$Q(z) = s(z)/s_R(z) , \tag{18}$$

where $s_R(z)$ is the total volume coefficient for Rayleigh scattering at altitude z. Note that

$$s(z) = s_R(z) + s_M(z) = \omega(z)\alpha(z) , \tag{19}$$

where $\alpha(z)$ is the extinction coefficient and $s_M(z)$ is the aerosol scattering coefficient, also referred to as the Mie scattering coefficient. It follows that the Mie scattering ratio is given by

$$s_M(z)/s_R(z) = Q(z) - 1 \tag{20}$$

The Mie scattering ratio also would be constant under conditions of complete aerosol mixing.

Profiles of $Q(z)$ derived from the extensive series of airborne optical measurements made by the Visibility Laboratory, reveal large variability depending upon the aerosol particle source strength and the nature of the convective and turbulent mixing processes. The problem is to model the essential characteristics of the $Q(z)$ profiles in a way that recognizes operational observing and forecasting limitations yet takes maximum advantage of existing capabilities. A prominent feature of the daytime aircraft soundings over inland areas is the marked tendency for $Q(z)$ to remain essentially constant with height within the surface haze layer, and also in the upper troposphere above the primary haze layer. It should be emphasized that the assumption of constant scattering ratio with height does not hold well for ground-based stable layers with little vertical mixing such as those associated with the nocturnal formation of fog. However, for application to problems of contrast transmittance in hazy atmospheres in the daytime following the dispersion of any surface inversion existing at sunrise, it is reasonable to employ a model consisting of two or more tropospheric layers of constant optical scattering ratio. Thus, the forecasting problem is reduced to the prediction of the altitude limits of the atmospheric layers and the scattering ratio within each layer.

Representation of $Q(z)$ with a simple model consisting of two tropospheric layers was tested (Johnson *et al.*, 1979) using data obtained from experimental flights with the instrumented aircraft in western Europe in the spring and fall of 1976 and again in the summer of 1977. The optical scattering ratio was assumed constant with altitude both in the primary low-level haze layer and in the relatively clear region aloft in the middle troposphere. An exponential decrease of scattering ratio with height was assumed in the transition layer between the top of the haze layer and the base of the upper troposphere layer. The depth of this intermediate transition layer was held constant at 300m, which was the approximate average transition zone depth for the measured profiles. However, the depth of the low-level haze layer was made a variable to be specified or predicted in operational practice from meteorological variables. Attenuation over slant paths between the surface and upper troposphere is, of course, sensitive to the depth of the haze layer, Z, as well as to the scattering ratios Q_l and Q_u in the primary (lower) haze layer and in the upper troposphere layer, respectively.

Processed data from the first three European deployments for experimental flights reaching an altitude of at least 3 km were used for the preliminary tests of the scattering ratio model. Each flight usually included scattering coefficient profile measurements with each of four spectral filters having peak wavelengths of 475, 550, 660 and 750 nm. The four profiles were measured sequentially over approximately a 2-hour period. Sample profile data are shown in Fig. 3-1 along with the model representations as determined by the method of least squares. The logarithmic (base e) rms specification error of the individual profile values of scattering ratio measured at 30m intervals is .15 (or approximately 15 percent rms error) for flight C-372 and .17 for flight C-390. The median logarithmic rms error of daytime profile representation by the single haze layer model was .20 for the 87 individual filter profiles (23 flights) in the test series.

Limitations of the simple 2-layer model representation of scattering ratio profile result primarily from occurrences of multiple haze layer structure rather than the lack of scattering ratio uniformity within a given haze layer. For example, both a dense haze layer near the ground and an intermediate haze layer of lesser density are evident in the third profile shown in Fig. 3-1. Flight C-418 was an early morning flight made over open farmland in northwestern Germany. Extension of the model to include definition of the multi-layered structure is required in such situations to significantly reduce the logarithmic rms specification error in this case, which was near 0.4 for the simple 2-layer representation of the profile. The computer code for the calculation of contrast transmittance has provision for the inclusion of as many atmospheric layers as warranted in complex situations when detailed information about the scattering ratio profile is available.

3.2 Specification of Haze Layer Depth

As summarized by Benkley and Schulman (1979), several techniques have been proposed for estimating boundary layer mixing depths for inland areas. Various models are available for the calculation of both the height of the nocturnal boundary layer which is dependent primarily upon radiational cooling processes and wind-shear turbulence, and the depth of the daytime mixed layer which is dependent primarily upon the vertical penetration of free convection arising from surface heating. Particularly in the daytime, the ambient temperature profile can be used to help identify the expected mixing layer depth and therefore the height of the low-level haze layer.

Simultaneous high-resolution profiles of optical scattering ratio and temperature measured by the instrumented aircraft were used to explore temperature lapse rate criteria for the specification of haze layer depth (Johnson *et al.*, 1979). The data base consisted of the same group of 23 flights (87 profiles) measured in western Europe that were used for preliminary tests of the scattering ratio model. Sample calculations of the temperature lapse rate profile and the corresponding scattering ratio profile are shown in Fig. 3-2. The lapse rate was calculated for overlapping 510m intervals spaced 30m apart, and is plotted at the base of the altitude interval over which it was calculated. The close relationship observed in this case between the base altitude of the stable layer and the depth of the primary haze layer is typical of most flights in the test series.

Tentative criteria were established from the initial tests to relate objectively the temperature lapse rate structure to haze layer depth. The stable layer was defined as the lowest altitude layer in which the lapse rate is less than

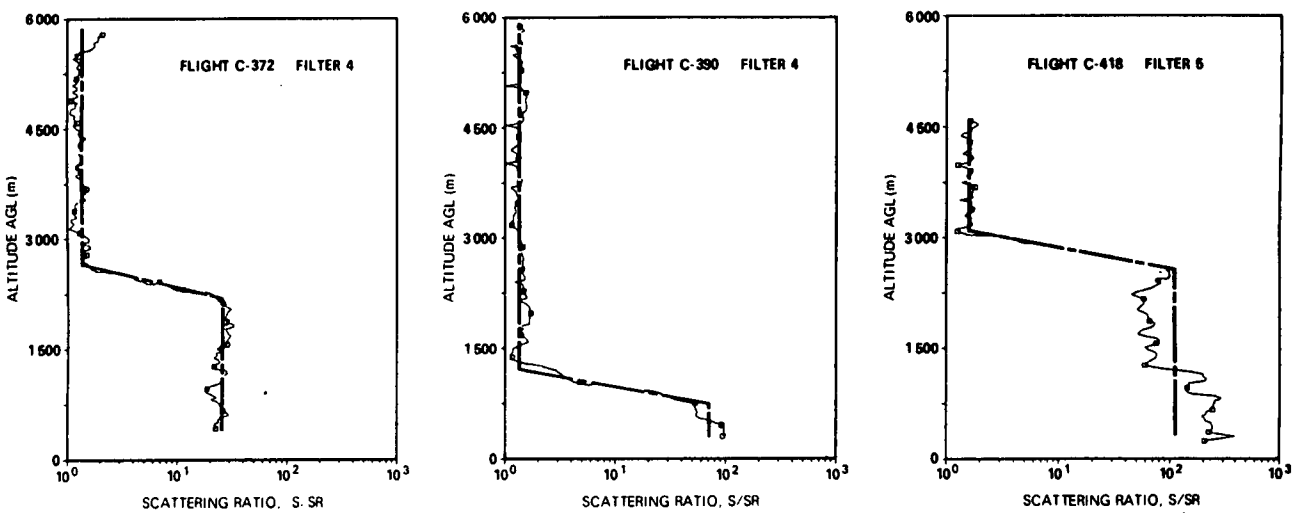

Fig. 3-1. Scattering ratio profiles as measured for flight C-372 (Soesterberg, Netherlands), flight C-380 (Rodby, Denmark) and flight C-418 (Alhorn, Germany). The heavy dashed line is the objective model representation of the profile. The nephelometer measurements were corrected for the effects of incomplete purging of the instrument.

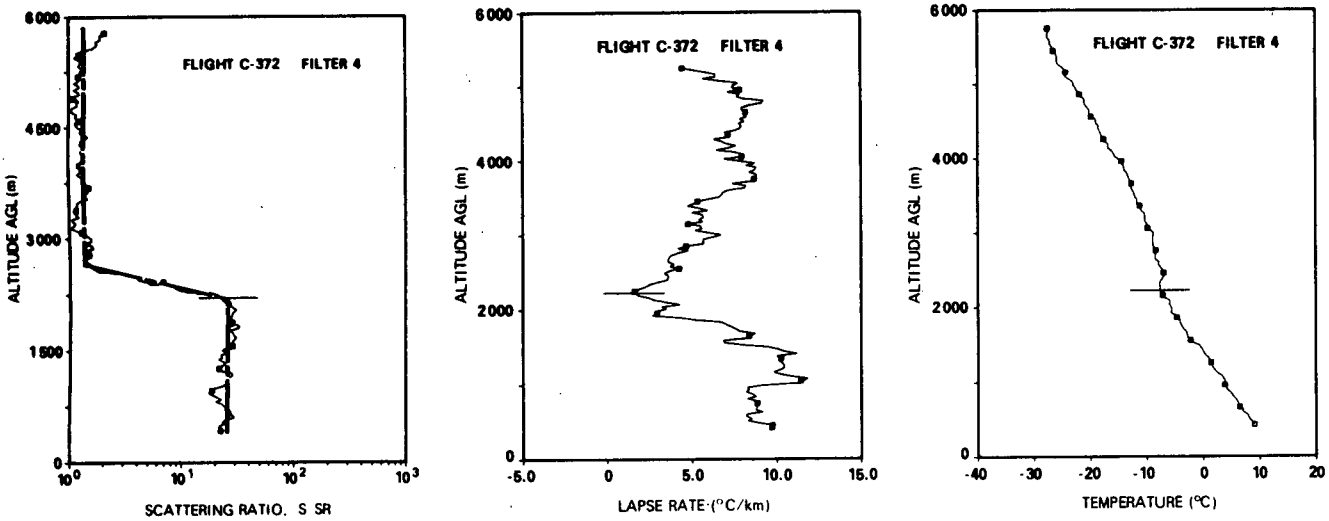

Fig. 3-2. Comparison of simultaneous profiles of optical scattering ratio, temperature and temperature lapse rate.

4.5°C km^{-1} (calculated over 500m vertical interval). The altitude of the haze layer top was assumed to be coincident with the altitude corresponding to the minimum value of lapse rate within this layer, as illustrated in Fig. 3-2. If no stable layer with an identifiable minimum of less than 4.5°C km^{-1} is observed, the altitude of the minimum lapse rate observed below 4 km in altitude was selected as the upper limit of the primary haze layer. These criteria are straight-forward except they leave undefined the case when a very low inversion or stable layer was present, and the base of the layer was below the lowest altitude sampled by the aircraft (usually 100m to 200m above ground level).

The correspondence between the haze layer depth, Z, and the estimate of Z given by the temperature lapse rate criteria stated above is illustrated by one example in Fig. 3-2. For purposes of the initial tests (Johnson *et al.*, 1979) the base of the thermally stable layer was calculated from the average of the temperature profiles (usually 4) measured by the instrumented aircraft within about a 2 hour period. Similarly, the value of Z was obtained by a simultaneous fit by the method of least squares to all of the corresponding profiles of $Q(z)$ as derived from the flight data for the same time period. For the test sample, the standard error of estimate of Z from the lapse rate criteria was 123m. The departures tended to be systematic in that the haze layer typically extends somewhat above the calculated base-height of the stable layer at low Z and somewhat below the calculated height when the haze layer is relatively deep. More information on the validation of the profile modelling approximations with the experimental aircraft measurements is given in Johnson *et al.* (1979).

3.3 Summary of Proposed Technique for the Specification of the Scattering Coefficient Profile in the Troposphere

The modelling techniques for estimating slant-path contrast transmittance will accept as input a much more detailed representation of the scattering coefficient profile than that given by the simple 2-layer troposphere model. The atmosphere may be divided into as many layers as warranted by available observations and forecasts, with each layer having a different but constant value of $Q(z)$. However, a general review of all published high resolution profiles of total volume scattering coefficient and temperature obtained from the many deployments of the instrumented C-130 aircraft in the United States and Europe and the results of the limited quantitative analysis based on a selected series of test data suggest the following:

(a) The simple 2-layer troposphere model with a single low-level haze layer of variable depth and a relatively clear troposphere aloft represents the vertical profile of optical scattering ratio with good approximation in most daytime situations encountered by the experimental aircraft operating under visual flight rules.

(b) A more complete haze-layer model is required for reasonable profile representation in conditions identified by the presence of a significant ground based stable layer with moderate to dense haze or fog in addition to an intermediate layer of lower haze density.

(c) In the absence of other measurements, the depth of the primary haze layer can be estimated effectively by temperature lapse rate criteria which identify thermally stable layers in the lower troposphere. The relevant stable layers usually are of sufficient depth and strength to be identified with conventional radiosonde observations. However, standard methods of processing the raw radiosonde measurements result in diminished resolution of temperature lapse rate structure and, on occasion, seriously limit the determination of mixing depth.

(d) To a good first approximation, the scattering mixing ratio can be assumed constant with height in the primary haze layer and again in the troposphere above

the transition zone. It follows, for example, that the average scattering ratio in the low-level haze layer may be estimated effectively by an observation or reliable forecast of scattering ratio at the base of the layer.

4. SINGLE SCATTERING PHASE FUNCTION REPRESENTATION

As discussed in Section 2, the component of directional path function generated by the scattering of direct solar radiation reaching the path is given by the product of the phase function for single scattering, the scattering coefficient and the solar irradiance. The phase function for single particle scattering depends in a complex way on the size distribution and refractive index of the aerosol particles and the wavelength of the incident light. In general, as the particle size increases with respect to the wavelength, the amount of energy scattered in directions close to that of the incident radiation increases markedly while the concomitant backscattering components decrease, resulting in larger asymmetry of the phase function. Since the total volume scattering coefficient varies systematically as the square or larger power of the particle radius depending upon the size parameter, we might expect that the total volume scattering coefficient or scattering ratio, $Q(z)$, might provide, through analytic representation, a good first approximation for the single scattering phase function. As discussed below, experimental evidence shows this to be true.

The approach used herein for model development was first to represent the single scattering phase function for Mie scattering $P_M(z,\beta)$ by two term Henyey-Greenstein (Irvine, 1968) functions as follows,

$$P_M(\beta,g_1,g_2,c) = c\,P_{HG}(\beta,g_1) + (1-c)P_{HG}(\beta,g_2)\,, \quad (21)$$

where

$$P_{HG}(\beta,g) = (1-g^2)/\,[\,4\pi(1-2g\cos\beta+g^2)^{3/2}\,]\,, \quad (22)$$

and the asymmetry factor, g, is given by

$$g = \frac{1}{2}\int_0^{\pi} P(\beta)\cos\beta\sin\beta\,d\beta\,. \quad (23)$$

The phase function for single scattering has the normalized form,

$$\int_{4\pi} P(z,\theta,\phi)\,d\Omega = 1 \quad (24)$$

In turn, the Henyey-Greenstein function parameters, $g_1(z)$, $g_2(z)$ and $c(z)$ are approximated as individual functions of the Mie scattering ratio, $Q(z)-1$, as described below.

The single scattering phase function for combined aerosol and molecular scattering is bounded by the Rayleigh phase function ($Q=1,g=0$) for a clear atmosphere and by a phase function corresponding to dense clouds or fog for very large $Q(z)$. Combined analysis of the asymmetry parameters (g_1,g_2,c), as derived from both a least-squares fit of the Henyey-Greenstein functions to the average phase functions measured by Barteneva (1960) and to the phase functions derived from Mie calculations using typical aerosol distributions in haze and fog, led to the following consistent set of empirical equations. The equations express the asymmetry parameters as a function of the Mie scattering ratio, $(Q-1)$, as follows:

for $1<Q<1000$

$$g_1(z) = .0539\ln[\,Q(z)-1\,] + .541\,, \quad (25)$$

$$g_2(z) = -.0442\ln[\,Q(z)-1\,] - .471\,, \quad (26)$$

for $Q\geq 1000$

$$g_1(z) = .913\,, \quad (27)$$

$$g_2(z) = -.776\,, \quad (28)$$

for $1<Q<64.7$

$$c(z) = -.007\,[\,\ln(Q(z)-1)\,]^2 + .07\ln[\,Q(z)-1\,] + .81\,, \quad (29)$$

and for $Q\geq 64.7$

$$c(z) = 0.98\,. \quad (30)$$

The asymmetry factor, g_M, for Mie scattering is given by

$$g_M(z) = c(z)g_1(z) + [\,1-c(z)\,]\,g_2(z)\,, \quad (31)$$

and the asymmetry factor for combined aerosol and molecular scattering is

$$g(z) = g_M(z)\,[\,Q(z)-1\,]/Q(z)\,. \quad (32)$$

Similarly, the single phase function for combined particle and air molecule scattering is given by

$$P(\beta,z) = \frac{P_R(\beta) + [\,Q(z)-1\,]\,P_M(\beta,z)}{Q(z)}\,, \quad (33)$$

where the theoretical Rayleigh phase function is

$$P_R(\beta) = 3(1+\cos^2\beta)/16\pi\,. \quad (34)$$

Independent evidence of the general applicability of the model estimates of $P(\beta)$ with respect to wavelength and altitude is given by a comparative study by Johnson *et al.*, (1979) of the directional scattering functions measured by the Visibility Laboratory airborne nephelometer and the Barteneva (1960) phase function measurements. In addition to the measurement of total volume scattering coefficient, the integrating nephelometer measured, separately, the directional scattering function at nominal scattering angles of 30° and 150° in four wavelength bands centered near 475, 550, 660, and 750 nm. The analysis by Johnson *et al.*, (1979) of the airborne data gathered by the Visibility Laboratory in Europe and the United States over all seasons indicates that the derived relationship between the average phase functions and the median scattering ratio for the individual asymmetry classes as measured by Barteneva (1960) holds well over all visible wavelengths and over all altitudes up to the highest levels sampled by the instrumented aircraft (usually near 6 km).

In Fig. 4-1, the phase function for single scattering, $P(\beta)$, that was calculated using the above system of equations is shown in comparison with sample calculations from Mie theory (Kattawar, 1975) and in comparison with the Barteneva measurements for a hazy atmosphere with a comparable scattering ratio. The representation of $P(\beta)$ with the system of two term Henyey-Greenstein functions, which are in turn related to $Q(z)$, are in good agreement with the Barteneva function but depart systematically in the range of the values extrapolated by Barteneva for scattering angles outside the actual range of the measurements, 0° to 16° and 164° to 180°. In comparison with the theoretical phase functions, the model calculations assuming $Q(z) = 26$ (equivalent surface visibility of about 10 km) compare closely with the phase function calculations based upon the Haze L particle size distribution of Deirmendjian (1969), and a assumed refractive index $m = 1.55-.00i$. The largest disparities are noted for scattering angles near 120° where the model calculations are higher, and near 180° where the model calculations are lower than the theoretical calculations.

A comparison of the model and theoretical calculations of $P(\beta)$ for a cloud case is shown in Fig. 4-2. The values of $P(\beta)$ calculated (Kattawar, 1975) using the indicated drop size distribution and refractive index are compared with the $P(\beta)$ calculated from the model assuming the value of Q is greater than 1000. Although an extension of model calculations to cloud situations yields reasonable definition of the general features of the $P(\beta)$ dis-

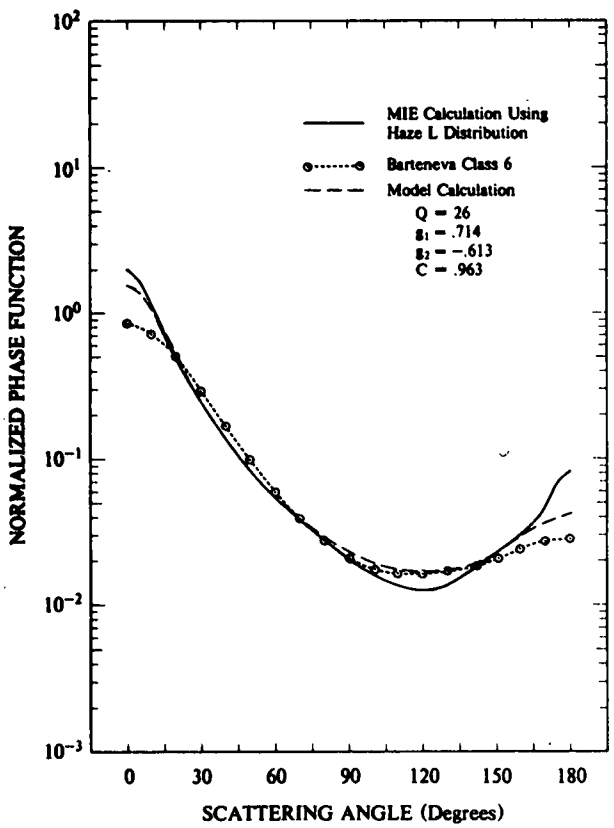

Fig. 4-1. Single scattering phase functions (a) calculated from Mie theory by Kattawar (1975) using Diermendjian (1969) Haze L distribution with a refractive index of 1.55 - 0.0i; (b) observed by Barteneva (1960) (class 6); and (c) calculated from Eqs. (25-34) for scattering ratio of 26.

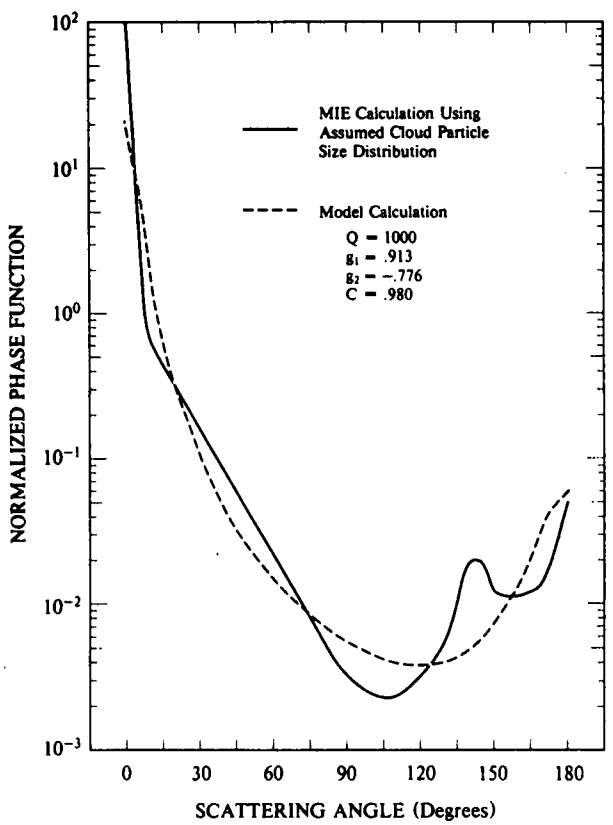

Fig. 4-2. Single scattering phase functions (solid line) calculated from Mie theory by Kattawar (1975) for cloud drop distribution $n = kr^6e^{-1.5r}$ and refractive index of 1.33 - 0.0i; and (dashed line) calculated from Eqs. (25-34) for scattering ratio of ≥ 1000.

tribution, important details typical of phase functions for fog, such as the prominent minimum near $\beta = 100°$ and the secondary maximum near 140°, are smoothed out by the representation with Henyey-Greenstein functions.

To the extent that more accuracy is desired and more complete information is available to define $P(z,\beta)$, the overall computer code for calculating path radiance and contrast transmittance was made general so that it will accept as input for each atmospheric layer any specified $P(z,\beta)$. However, in the absence of substantive information other than an estimate of $Q(z)$, calculation of $P(z,\beta)$ from the system of model equations is recommended. Additional evidence of the applicability of the model for estimating $P(z)$ from $Q(z)$ is given by the comparisons of measured and computed sky and terrain radiances that are discussed in the following section.

5. COMPUTER APPLICATION OF MODELLING TECHNIQUES

The procedures for the calculation of sky and terrain radiances were designed to take advantage of all relevant input data. In particular, the techniques for modelling the scattering coefficient and scattering phase function profiles and the procedures for radiative transfer calculation are optional and may be replaced by more detailed data or by other modelling techniques. A summary of the computational steps in the assembled program and a listing of the input data and the resultant products are given in Appendix B.

As input to the radiance and contrast transmittance computations, one may introduce as many atmospheric layers as warranted by the completeness of the observations and forecasts. Minimum input data for each layer are the altitude limits, the average scattering ratio and the average single scattering albedo. A listing of the specific input data for the model calculations described below is given in Appendix C.

5.1 Model Results and Comparisons with Measured Data

The overall effectiveness of the modelling techniques described in Sections 2, 3 and 4 was tested through direct comparisons of sky and terrain radiances measured by the airborne scanning radiometer and the radiance distributions calculated with the model. A series of comparative results are shown in Figs. 5-1 - 5-8. They illustrate some of the model performance characteristics at selected altitudes for several flight profiles covering a range of low-level haze conditions, wavelength intervals and solar zenith angles.

Comparative results for flight C-466, conducted over a rural area in northwestern Germany, are shown in Figs. 5-1 and 5-2 for the narrow band blue filter with a central wavelength of 475 nm. This midday flight was made under conditions of isolated patches of middle clouds and scattered thin cirrus. Moderate haze extended to 1.3 km and the surface visibility was near 15 km. The solar zenith angle averaged about 44 degrees. The $\theta > 90°$ segments of the observed radiance distribution, looking downward from an altitude of 200m, shown in Fig. 5-1, reflect significant fluctuations that are caused by changes in the inherent reflectance of the underlying surface, which varied from dark woods to open fields. As shown in Fig. 5-2, the influence of the surface reflectance variations on the radiance is greatly smoothed by the effects of the intervening atmosphere as measured from an altitude of 6 km by the scanning radiometer. The 5-degree field of view of the radiometer also results in smoothing. The measured directional radiance values at 6 km were subject to significant stray light error for viewing angles near the sun and are not shown in the comparison. A prominent characteristic of the radiance distribution at 6 km is the bright horizon sky radiance which in this case had comparable brightness in the upsun ($\phi = 0°$) and downsun ($\phi = 180°$) azimuthal directions.

Comparative results for a Winter flight with low altitude sun conditions are shown in Figs. 5-3 and 5-4. Flight C-401 was made in the early afternoon over open farmland and occasional woods in northwestern France. A very light haze layer extended to an altitude of 1400m with a surface visibility of 30 to 40 km. Scattered cirrus and low-level cumulus clouds were present in the area during the period of measurement. The results in this case are for the broad band photopic filter with a central wavelength of 550 nm. The correspondence in measured and model radiance is good at both levels except for the tendency to overestimate the radiance for zenith viewing angles near 180° (directly downward below the aircraft).

The comparative results for a case with thick haze conditions is shown in Figs. 5-5 - 5-8. For flight C-469, the low-level haze layer extended to altitude 1000m with the surface visibility in the range 5 to 8 km. A second haze layer of somewhat lower density with the base at 1200m and top 1500m persisted throughout the period of measurement. It was an afternoon flight made over the central Netherlands. The underlying terrain features were predominantly green fields with occasional brown fields, woods and small towns. The flight track was adjusted somewhat during the afternoon to remain in advance of a broken to overcast layer of cumulus clouds located immediately to the west and north of the track. Shown for comparison in this case are the results for the two filters with central wavelengths near the upper and lower limits of the visible spectrum; the blue filter (475 nm) measurements are shown in Figs. 5-5 and 5-6, and the near infrared filter (750 nm) in Figs. 5-7 and 5-8.

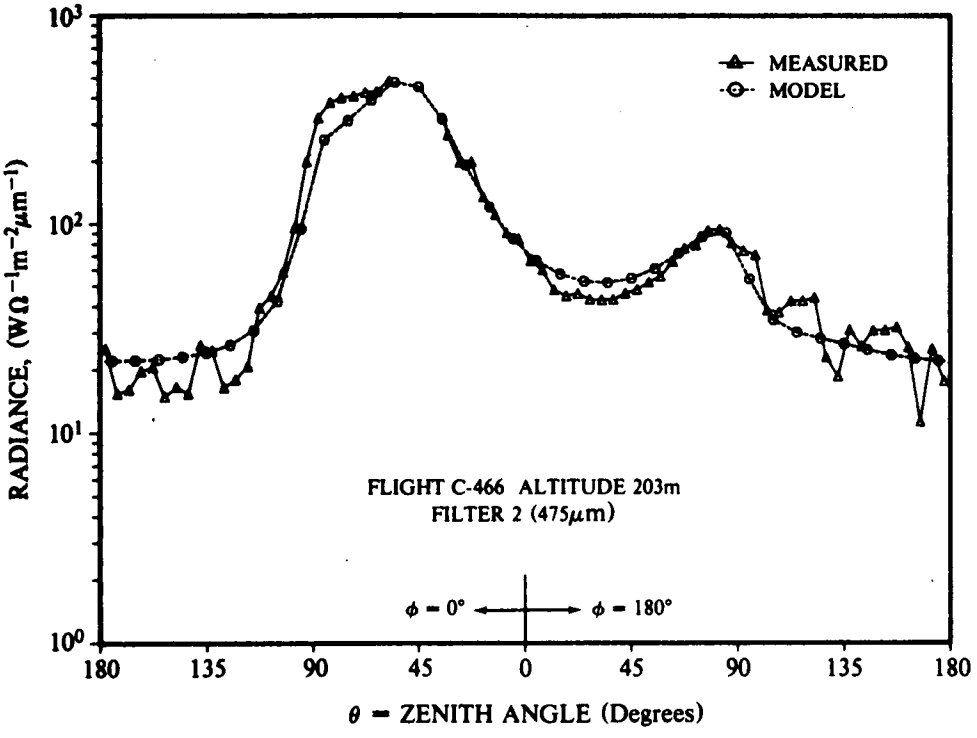

Fig. 5-1. Comparison of measured and calculated sky and terrain radiance distributions at 200 m for flight C-466 (Meppen, Germany). The solar zenith angle is 48 deg.

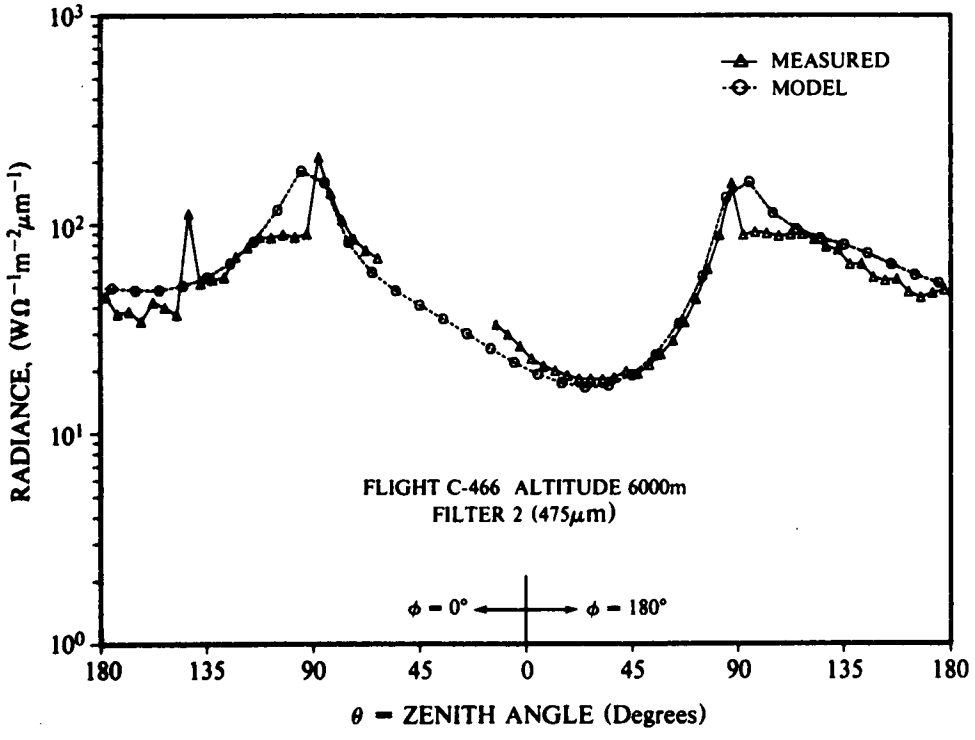

Fig. 5-2. Comparison of measured and calculated sky and terrain radiance distributions at 6000 m. The solar zenith angle is 41 deg.

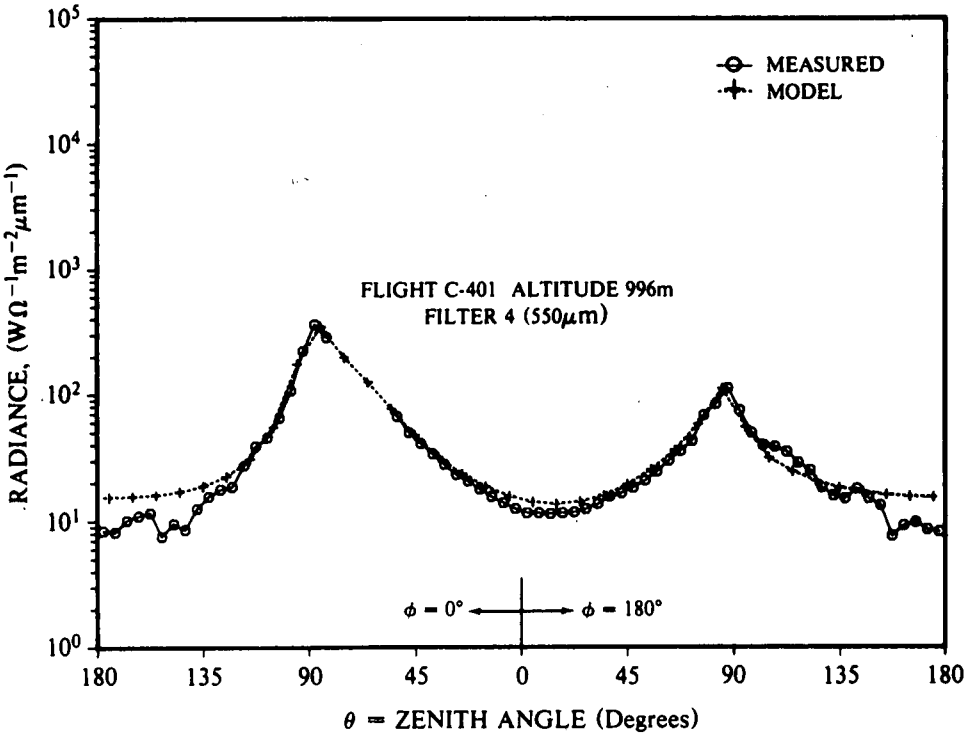

Fig. 5-3. Comparison of measured and calculated sky and terrain radiance at altitude 996m for flight C-401 (Bruz, France). The solar zenith angle us 72 deg.

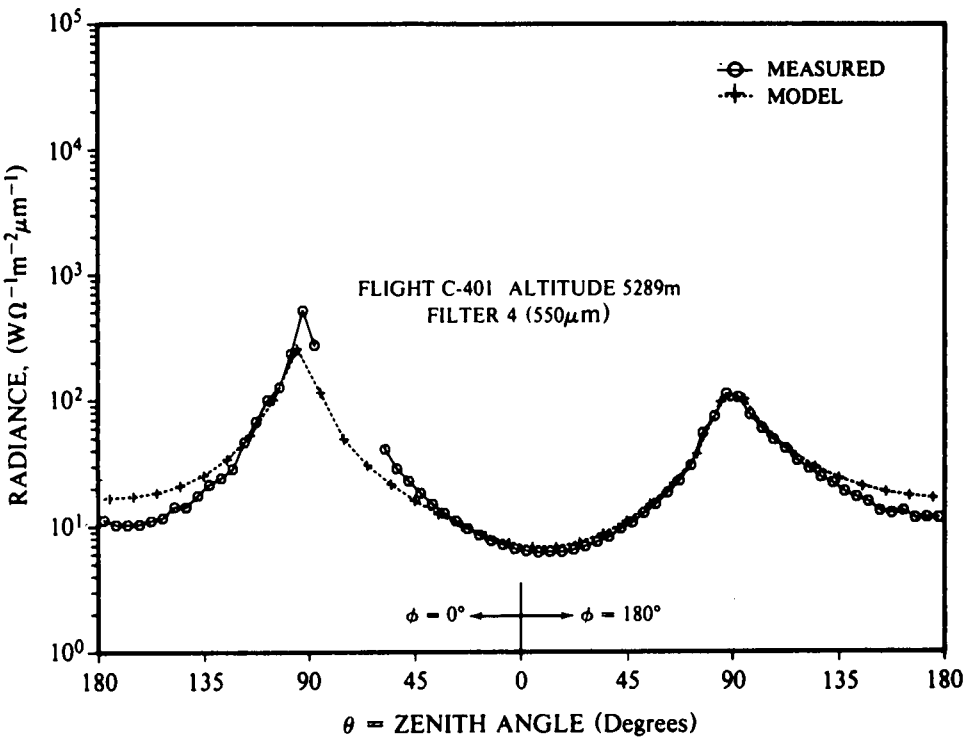

Fig. 5-4. Same as Fig. 5-3 except that the altitude is 5290m and the solar zenith angle is 76 deg.

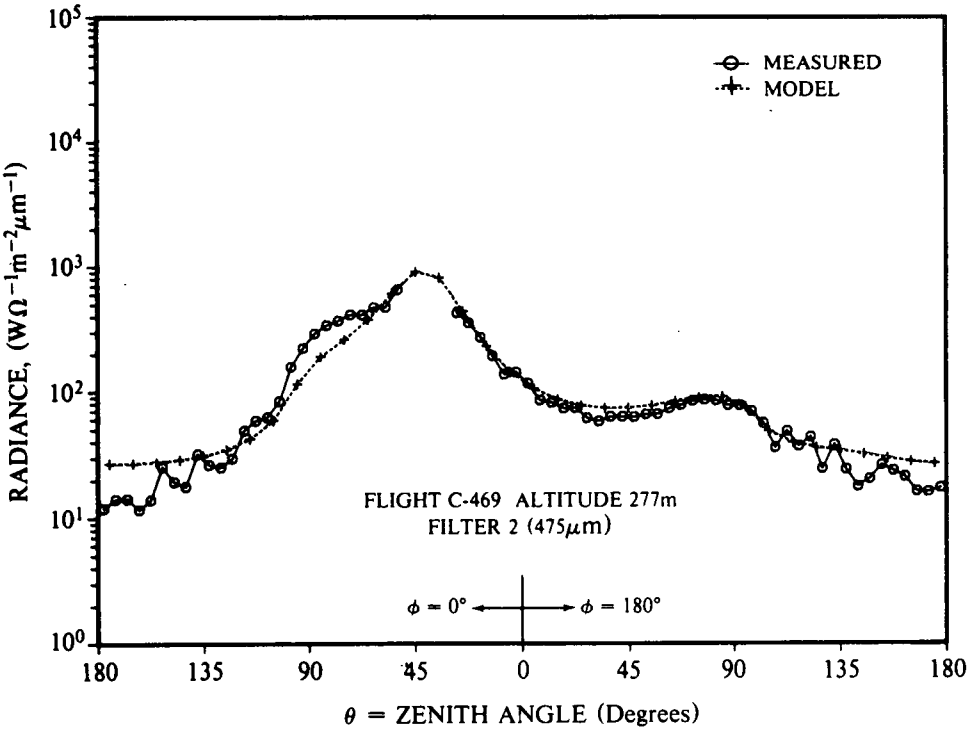

Fig. 5-5. Comparison of measured and calculated sky and terrain radiance at altitude 277m, Filter 2 (475 nm), for flight C-469 (Soesterberg, Netherlands). The solar zenith angle is 40 deg.

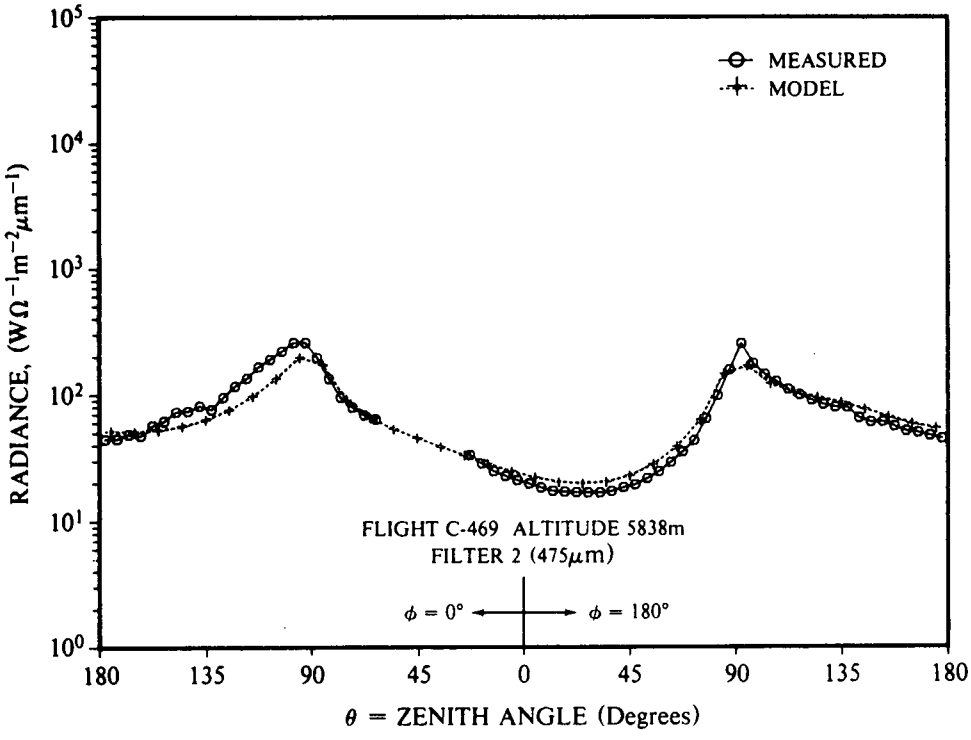

Fig. 5-6. Same as Fig. 5-5 except that the altitude is 5838m and the solar zenith angle is 44 deg.

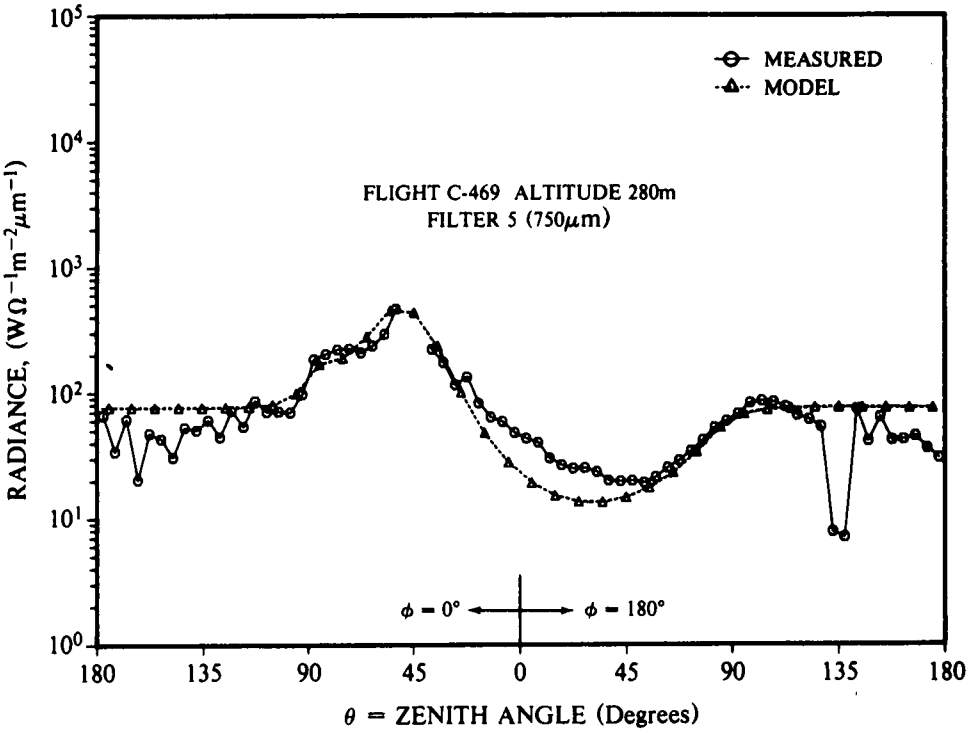

Fig. 5-7. Same as Fig. 5-5 except it is for Filter 5 (750 nm), and the altitude is 280m and the solar zenith angle is 48 deg.

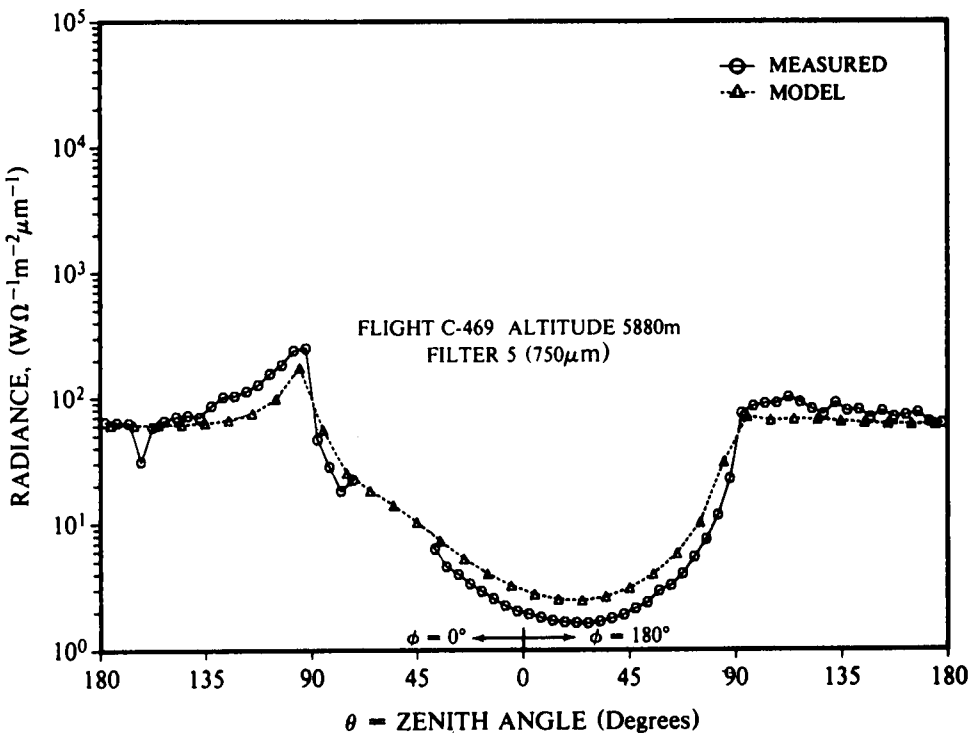

Fig. 5-8. Same as Fig. 5-7 except the altitude is 5880m and the solar zenith angle is 57 deg.

6. SENSITIVITY OF SPECTRAL CONTRAST TRANSMITTANCE TO SELECTED CHANGES IN PHYSICAL PARAMETERS

Systematic model calculations were made to illustrate the effects of typical variations in physical parameters upon the slant path contrast transmittance and the corresponding range of object detection. For this purpose, a two-layer atmosphere was assumed, consisting of a primary haze layer of varying optical thickness and single scattering albedo, and an overlying upper troposphere-stratosphere layer of relatively clear air with a constant optical scattering ratio of 1.3 and a single scattering albedo of 0.97. The trial calculations were carried out for an assumed wavelength of 550 nm. The responses in contrast transmittance to parameter changes would be qualitatively similar for other visible wavelengths but would show systematic quantitative differences for the same aerosol loading in the haze layer because of the wavelength dependence of both the total optical depth and the single scattering phase function.

Results are shown for a range of haze layer depths, aerosol concentrations and absorption, and for selected values of surface reflectance and solar zenith angle. The parameters are varied individually while holding each of the other variables constant and equal to their values for the assumed reference atmospheres given in Appendix C, which are in general representative of clear sky conditions observed in the summer season in northern Germany. The first two sets of calculations, Sections 6.1 and 6.2, were based upon reference atmosphere "A". The vertical extent of the haze layer for this reference atmosphere was assumed to be 3 km except that a few comparative calculations were made also for an assumed haze layer top at 500m altitude while holding the overall optical thickness the same as for the 3 km case. The third set of trial results (Section 6.3) were based upon reference atmosphere "B" (Appendix C), with the haze layer extending to 1.3 km and with a single scattering albedo of .83 and an optical scattering ratio of 16.

6.1 Object at the Earth's Surface and the Sensor at 6 Km

From Eq. (4), the contrast transmittance, $T_c = C_r/C_o$, of a downward path of sight to an object at the earth's surface is given by the product of the path beam transmittance, T_r, and ratio of the inherent background radiance of the surrounding terrain and the apparent background radiance as measured at the sensor altitude, ${}_bL_o/{}_bL_r$. It follows that the contrast transmittance decreases with an increase in the optical thickness of the viewing path in concert with both a decrease in $T_r(z,\theta)$ and an increase in the path radiance, L_r^*, generated by the enhanced aerosol particle scattering. For the case with the object at the surface and the sensor at 6 km, the responses of T_c to changes in optical thickness and to changes in the cosine of the zenith viewing angle are shown in Fig. 6-1. Since we have assumed that the surface reflectance obeys Lambert's law, the asymmetry of T_c in the upsun and downsun viewing directions is small. Except for viewing angles near the horizon, the calculated T_c from the surface to 6 km decreases more or less in direct proportion to the increase in slant path distance.

For diagnostic purposes let us define an arbitrary target acquisition range (TAR) where the contrast transmittance reduces to 10 percent. Illustrated in Fig. 6-2 are the calculated changes in TAR that correspond to selected changes in the physical variables. Again we assume a target located at the earth's surface and a sensor altitude of 6 km. The calculations were made for an azimuth viewing angle of 180° (downsun). The calculated TAR for the reference atmosphere is 13.5 km. Comparing responses of the TAR to the departures of the individual parameters from their values given by the reference atmosphere, we note that a 25 percent increase in TAR is associated with about a 25 percent decrease in the optical thickness of the haze layer. On the other hand about a 50 percent increase in optical thickness is required for a 25 percent decrease in TAR. The dotted line shown in Fig. 6-2 for the relationship of TAR with optical thickness depicts the calculated TAR for an haze layer top at 0.5 km in lieu of the 3 km altitude assumed for the reference atmosphere. Notice that the TAR differs only by approximately 15 percent for a haze layer with the greatly reduced vertical extent but with increased extinction so as to yield the same optical thickness.

Figure 6-2b shows that changes in ln TAR are directly proportional to the changes in the cosine of the solar zenith angle. For example, a decrease in solar zenith angle of 12 degrees results in about a 25 percent increase in TAR for the reference atmosphere. Notice also (Fig. 6-2d) that a 25 percent decrease in TAR is associated with an increase in haze layer absorption from the small amount associated with clear remote atmospheres (single scattering albedo = 0.97) to the large amount corresponding to urban atmospheres (single scattering albedo = 0.63).

For objects viewed against a terrain background, the TAR has a significant direct dependence upon the surface reflectance. For example (Fig. 6-2c), the calculated TAR decreases by 25 percent as the surface reflectance changes from the value associated with a brown field (0.10) to a value representative of a grass field (0.06).

6.2 Object at 6 Km and the Sensor at Ground Level

Diagnostic model calculations of T_c and TAR are shown in Fig. 6-3 and 6-4 for an object at 6 km when viewed against a sky background from the earth's surface. The reference atmosphere and selected changes to the reference atmosphere are the same as for the sensitivity analysis described in the preceding paragraphs. In contrast with downward paths of sight, the calculated contrast transmittance of upward paths have large asymmetry in the upsun and downsun directions because of the enhanced path radiance generated by the increased scatter-

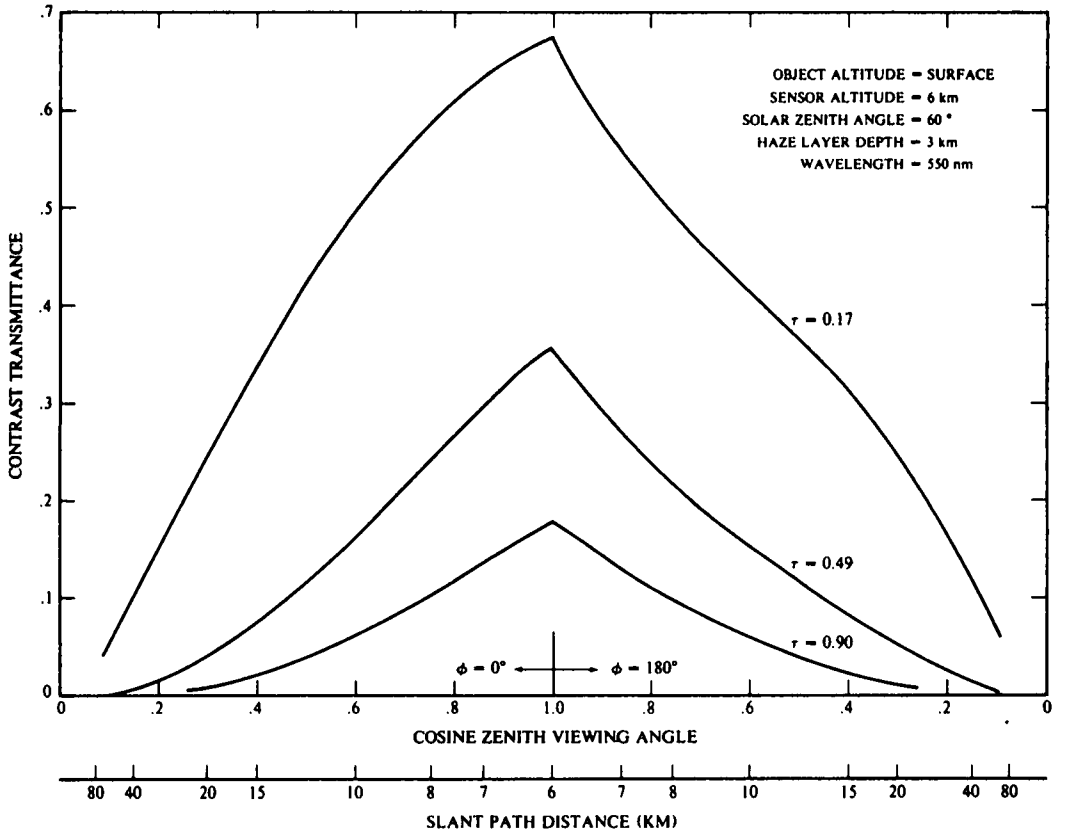

Fig. 6-1. Diagnostic calculations of contrast transmittance as a function of zenith viewing angle for a target viewed against a terrain background. Values of τ are total atmosphere optical depth.

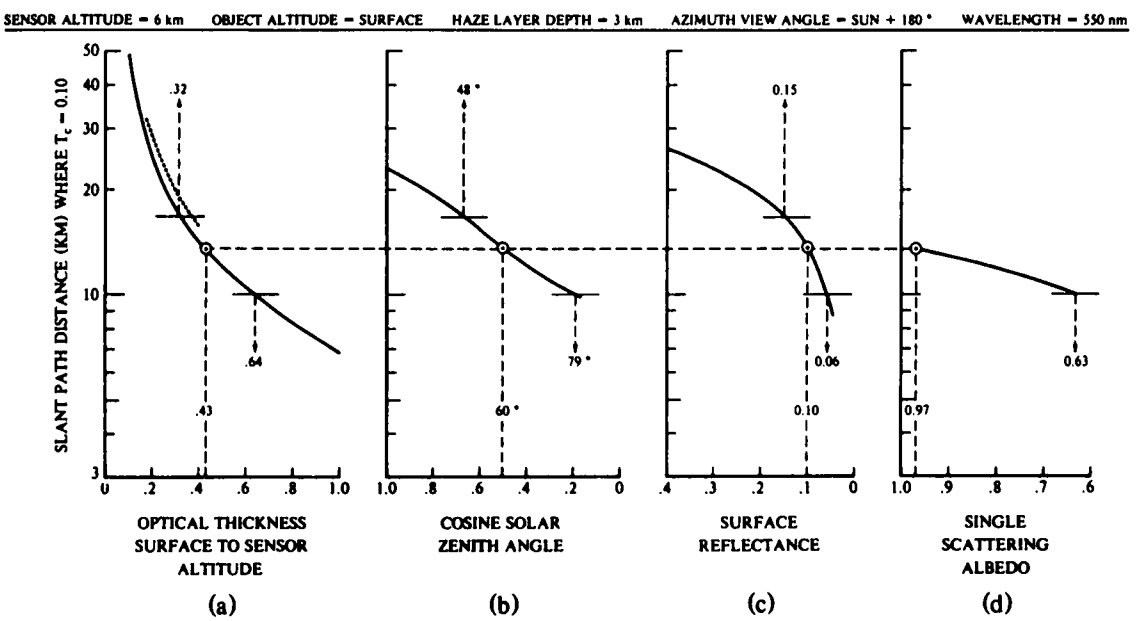

Fig. 6-2. Variations in target acquisition range (T_c = 0.10) associated with departures of selected parameters from the assumed reference atmosphere values. The horizontal dashed line denotes parameter values for this reference atmosphere. The horizontal bars identify a change of ±25 percent from the slant path distance where T_c = 0.10 for the reference atmosphere, *e.g.* 13.5 ±3.4 km.

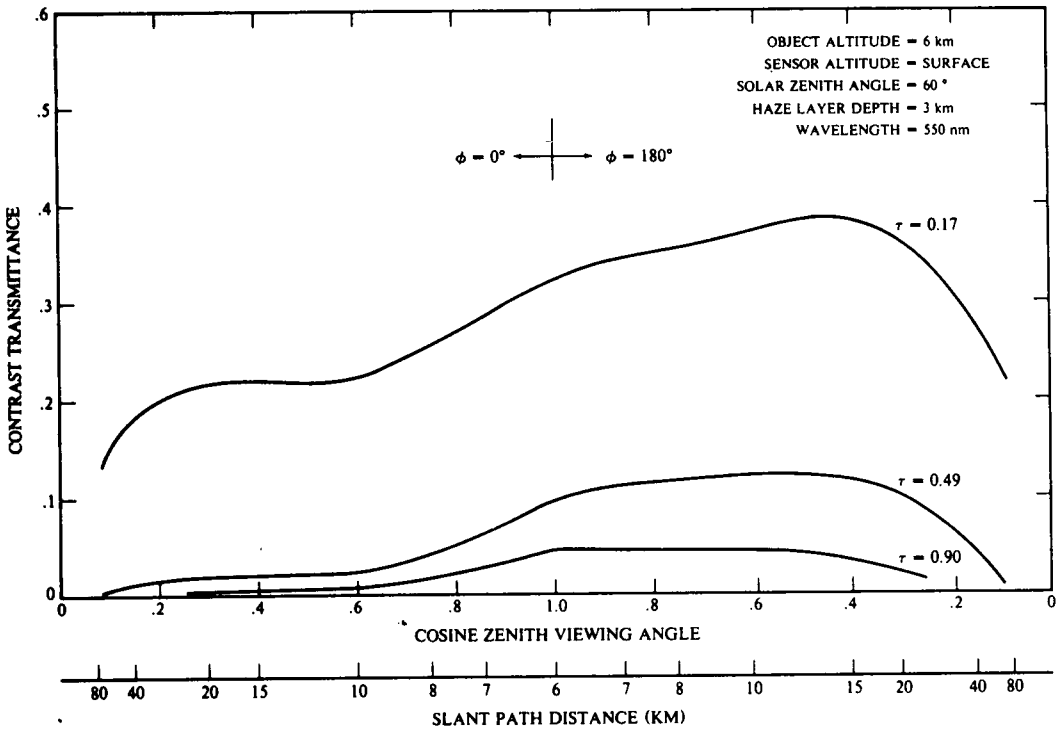

Fig. 6-3. Same as Fig. 6-1 except for a target viewed against a sky background.

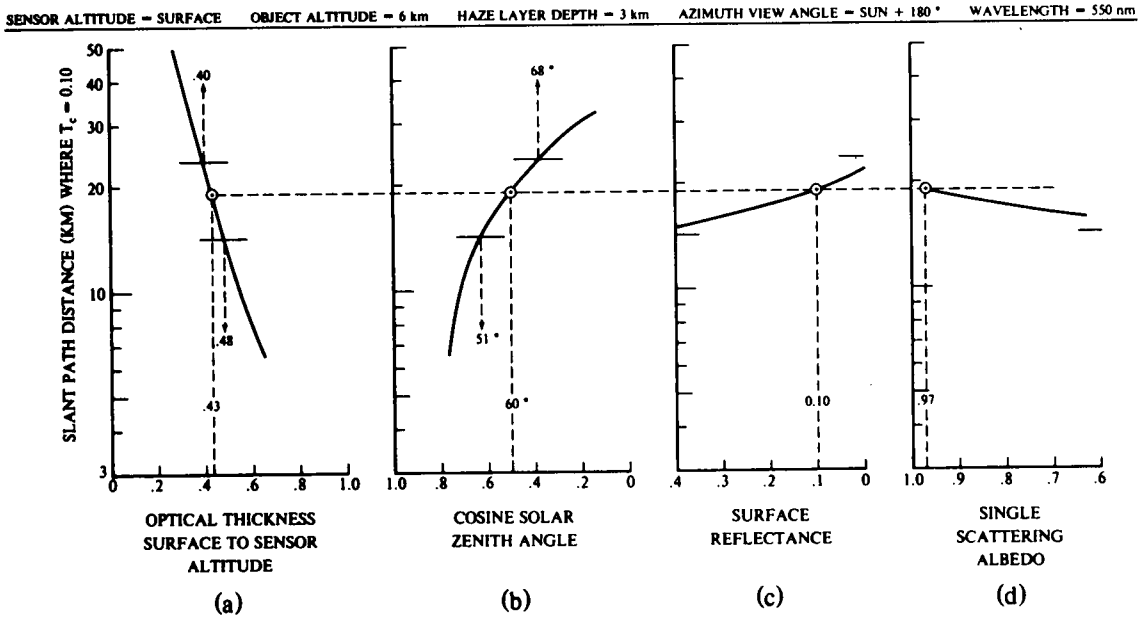

Fig. 6-4. Same as Fig. 6-2 except for a target viewed against a sky background.

ing of sunlight at forward scattering angles. As shown in Fig. 6-3, the calculated T_c for $\phi = 0°$ is less than 10 percent for all zenith angles when the total optical depth is 0.5 or larger. In the downsun direction ($\phi = 180°$), T_c has only a modest variation with zenith viewing angle for angles less than about 70°.

A strong dependence of target acquisition range in the downsun direction upon the optical thickness of the haze layer is evident in the results shown in Fig. 6-4a. A change in thickness of only 10 percent, holding other parameters of the reference atmosphere constant, results in about a 25 percent change in TAR. A marked sensitivity of the TAR to changes in solar zenith angle is also found, (Fig. 6-4d). The observed decrease in TAR with an increase in solar altitude stems from the associated increase in the path radiance. In comparison with the results shown in Fig. 6-2, the TAR for objects viewed against a sky background show significantly less response to changes in the single scattering albedo (Fig. 6-4d) of the haze layer and changes in surface reflectance (Fig. 6-4c).

6.3 Object at the Surface and the Sensor at 20 Km

The third and last set of trial calculations differs from the previous two in that a different reference atmosphere (REF-B in Appendix C) was assumed. The haze layer is more shallow, extending to 1.3 km, and the scattering ratio and single scattering albedo in the haze layer are 16 and 0.83 respectively. With the assumed sensor altitude of 20 km, the viewing path has a long segment through the relatively clear region in the lower stratosphere and upper troposphere. Yet another departure from the previous calculations is that the target at ground level is viewed in the upsun rather than the downsun direction.

The calculated slant range corresponding to 5 percent apparent contrast (contrast transmittance of 10 percent) for the reference atmosphere and for specific changes in the individual parameters of the atmosphere are shown in Fig. 6-5. We note, for example, that each of the following parametric changes in the reference atmosphere result in a decrease in the slant path distance corresponding to 5 percent contrast transmittance in the range of 19 to 25 percent:

a. 50 percent increase in haze layer depth
b. Factor of 5 increase in the aerosol scattering ratio in the upper troposphere
c. Increase in haze layer absorption corresponding to a change in single scattering albedo from .83 to .63
d. Increase in solai zenith angle from 50 to 60 deg

It should be emphasized that the results described in this section are specific only for the conditions imposed on the trial calculations. However, these examples provide some insight into the changes in image transmittance characteristics that are associated with typical changes in the environment.

7. SUMMARY COMMENTS

The techniques developed during the course of the experimental optical measurement and analysis program

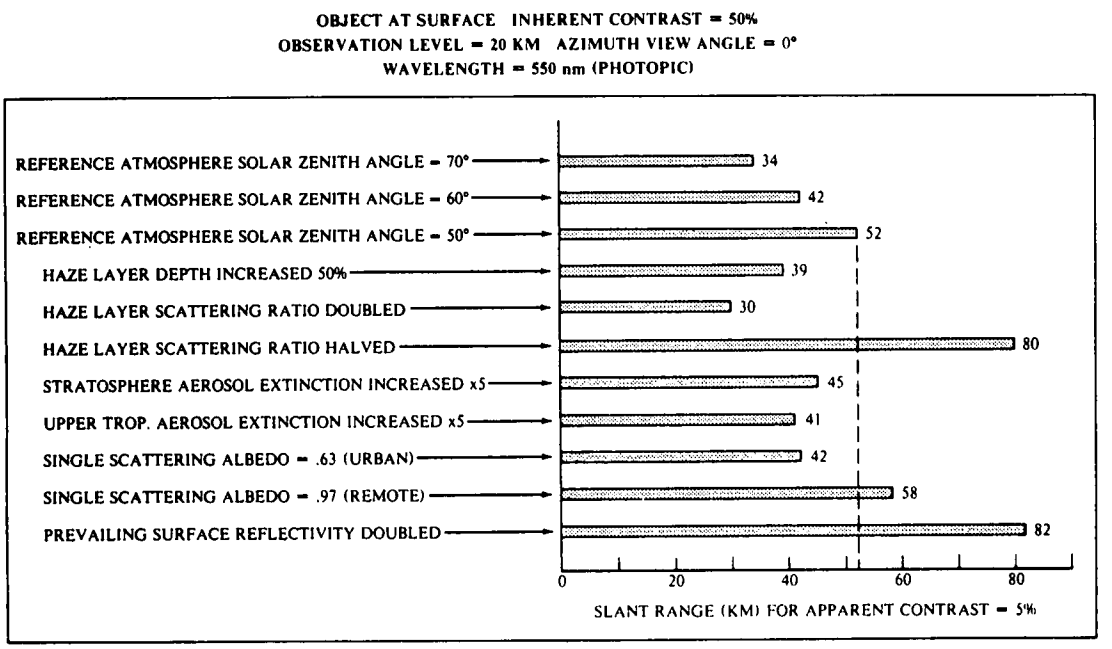

Fig. 6-5. Comparison of the slant range corresponding to apparent contrast of 5 percent for reference atmosphere (Ref. B, Appendix C) and selected changes in the reference atmosphere.

can provide relatively fast and consistent estimates of optical atmospheric properties over any slant path, as a function of wavelength in the visible spectrum. To the extent that a climatological data base of conventional meteorological observations exists, the techniques in their present form can be used to estimate readily the frequency distributions of such quantities as spectral contrast transmittance, as a function of location and season.

Refinements in the modelling approximations are being made as validation tests and experiments continue. Results to date indicate that further parameterization of selected components of the model can be made which will improve computational efficiency and at the same time retain the capability to take advantage of all relevant observing and forecasting information. A realistic goal is to employ the computer model as part of a data acquisition and microprocessing system for real time estimates of image transmission properties. Additional experiments are planned to examine further the tradeoffs between the type, accuracy, frequency and density of optical/meteorological observations and the reliability of the estimates of spectral contrast transmittance.

8. ACKNOWLEDGEMENTS

I would like to express appreciation to Eric Shettle of the Air Force Geophysics Laboratory for his guidance on model development and for his constructive comments on the presentation of the results. I also wish to thank Richard Johnson and Jacqueline Gordon of the Visibility Laboratory for their many helpful suggestions on the development of modelling techniques and their validation, and to thank Nils Persson of the Visibility Laboratory, who carried out the extensive computer programming and data processing portion of the research program.

9. REFERENCES

Barteneva, O. D. (1960), "Scattering Functions of Light in the Atmospheric Boundary Layer," Bull. Acad. Sci. U.S.S.R., Geophysics Series, 1237-1244.

Benkley, C. W., and L. L. Shulman (1979), "Estimating Hourly Mixing Depths from Historical Data", J. Appl. Meteor., *18*, 772-780.

Deirmendjian, D. (1969), "Electromagnetic Scattering on Spherical Polydispersions", Elsevier, New York.

Duntley, S. Q., A. R. Boileau, and R. W. Preisendorfer (1957), "Image Transmission by the Troposphere I", J. Opt. Soc. Amer., *47*, 499-506.

Gordon, J. I. (1969), "Model for a Clear Atmosphere", J. Opt. Soc. Am. *59*, 14-18.

Irvine, W. M. (1968), "Multiple Scattering by Large Particles II Optically Thick Layers", Astrophys. J., 152, 823-834.

Johnson, R. W., W. S. Hering, J. I. Gordon, B. W. Fitch and J. E. Shields (1979), "Preliminary Analysis and Modelling Based Upon Project OPAQUE Profile and Surface Data," University of California, San Diego, Scripps Institution of Oceanography, Visibility Laboratory, SIO Ref. 80-5, AFGL-TR-79-0285. NTIS, ADB 052 172L.

Joseph, J. H., W. J. Wiscombe, and J. A. Weinman (1976), "The delta-Eddington Approximation for Radiative Flux Transfer", Atmos. Sci., *33*, 2452-2459.

Kattawar, G. W. (1975), "A Three-Parameter Analytic Phase Function for Multiple Scattering Calculations", J. Quant. Spectrosc. Radiant. Transfer, *15*, 839-849.

Lenoble, J. (1977), "Standard Procedures to Compute Radiation Transfer in a Scattering Atmosphere", Working Group Report, Radiation Commission, International Association of Meteorology and Atmospheric Physics, 125p.

Shettle, E. P., and J. A. Weinman (1970), "The Transfer of Solar Irradiance Through Inhomogeneous Turbid Atmospheres Evaluated by Eddington's Approximation", J. Atmos. Sci., *27*, 1048-1055.

APPENDIX A

DERIVATION OF THE COMPONENT OF PATH RADIANCE DUE TO DIRECTIONAL SCATTERING OF DIFFUSE RADIANCE USING THE DELTA-EDDINGTON APPROXIMATION

The following derivation of Eq. (13) in Section 2.1 was provided by Mr. Eric P. Shettle of the Optical Physics Laboratory, Air Force Geophysics Laboratory. The equations referenced in the derivation are designated by number as given in Section 2 of this paper.

Substituting Eq. (12) into the last term of Eq. (6) we have,

$$\int\int_{4\pi} L(z,\theta',\phi')P(z,\beta)s(z)d\Omega' = s(z)\int_0^{2\pi}\int_{-1}^{+1} L_D(z)P_D(z,\beta)d\mu'd\phi' + s(z)\int_0^{2\pi}\int_{-1}^{+1}\mu' L_{D'}(z)P_D(z,\beta)d\mu'd\phi' , \quad (A.1)$$

where $\mu' = \cos\theta'$, and $d\Omega' = d\mu'd\phi'$. Using Eq. (7) in the first term on the right hand side of Eq. (A.1) and integrating over ϕ' we have,

$$s(z)\int_0^{2\pi}\int_{-1}^{+1} L_D(z)P_D(z,\beta)d\mu'd\phi' = \frac{s(z)L_D(z)}{2}\int_{-1}^{+1}[2f'\delta(\mu-\mu') + (1-f')(1+3g'\mu\mu')]d\mu' , \quad (A.2)$$

where $\cos\beta = \mu\mu' + \sin\theta\sin\theta'\cos(\phi-\phi')$

and $\delta(1-\cos\beta) = 2\pi\delta(\mu-\mu')\delta(\phi-\phi')$.

Since

$$\int_{-1}^{+1} 2f'\,\delta(\mu-\mu')d\mu' = 2f' \quad (A.3)$$

and

$$\int_{-1}^{+1}(1-f')(1+3g'\mu\mu')d\mu' = 2(1-f') , \quad (A.4)$$

Eq. (A.2) reduces to

$$s(z)\int_0^{2\pi}\int_{-1}^{+1} L_D(z)P_D(z,\beta)d\mu'd\phi' = s(z)L_D(z) . \quad (A.5)$$

Using Eq. (7) in the last term of Eq. (A.1) and integrating over ϕ' we have

$$s(z)\int_0^{2\pi}\int_{-1}^{+1}\mu' L_{D'}(z)P_D(z,\beta)d\mu'd\phi' \quad (A.6)$$

$$= \frac{s(z)L_{D'}(z)}{2}\int_{-1}^{+1}\mu'[\,2f'\delta(\mu-\mu') + (1-f')(1+3g'\mu\mu')\,]d\mu' ,$$

and integrating over μ' we have

$$s(z)\int_0^{2\pi}\int_{-1}^{+1}\mu' L_{D'}(z)P_D(z,\beta)d\mu'd\phi' = s(z)L_{D'}(z)\mu[\,f' + (1-f')g'\,] . \quad (A.7)$$

Substituting Eqs. (A.5) and (A.7) into Eq. (A.7) and from Eq. (11), $[\,f' + (1-f')g' = g\,]$, the expression for the diffuse component of the path function is given by

$$\int\int_{4\pi} L(z,\theta',\phi')P(z,\beta)s(z)d\Omega' = s(z)\,[\,L_D(z) + gL_{D'}(z)\cos\theta\,] . \quad (A.8)$$

Also:
(Eq. 13, Section 2.1)

APPENDIX B

SUMMARY OF INPUT DATA, COMPUTATION STEPS AND RESULTANT DATA

B.1 General Input Data

B.1.1 Number of atmospheric layers

B.1.2 Representative wavelength (μm)

B.1.3 Extraterrestrial solar (lunar) irradiance ($w/m^2\mu m$)

B.1.4 Rayleigh optical depth for top layer for $\lambda = .55\mu m$ (unless otherwise specified, set equal to .0258 for layer base altitude of 10 km).

B.1.5 Solar zenith angles (deg.)

B.1.6 Zenith viewing angles (deg.)

B.1.7 Scattering angles between viewing path and sun (deg., max. 10).

B.1.8 Average reflectance of underlying surface and reflectance of background in the vicinity of target if different than the average reflectance.

B.2 Input Data Each Layer

B.2.1 Base altitude (km)

B.2.2 Scattering mixing ratio

B.2.3 Single scattering albedo

B.3 Computation Steps

B.3.1 Compute Rayleigh atmosphere optical thickness for each layer

B.3.2 Compute total optical thickness for each layer.

B.3.3 Compute optical depth for the base of each layer.

B.3.4 Compute single scattering phase function and asymmetry factors for each layer. (These parameters may be specified if desired in lieu of the use of model algorithms).

B.3.5 Transform optical depth, single scattering albedo, and asymmetry factor in accordance with delta-Eddington approximation.

B.3.6 Compute path function distribution for the base of each sub-layer (each layer is divided equally into 2 sub-layers).

B.3.7 Compute path radiance distribution for each sub-layer.

B.3.8 Compute path transmittance distribution for each sub-layer.

B.3.9 Compute sky/terrain radiance distribution at sub-layer boundaries.

B.3.10 Compute slant path contrast transmittance of selected paths.

B.4 Output Tables and Data

B.4.1 Single scattering phase function, $P(z,\beta)$, as calculated or specified for each layer.

B.4.2 Path radiance, $L^*(z,\theta,\beta)$, for each sub-layer and each solar zenith angle, θ_s.

B.4.3 Path transmittance $T_r(z,\theta)$ for each sub-layer.

B.4.4 Sky radiance, $L_r(z,\theta,\beta)$, for $0° \leqslant \theta \leqslant 85°$ for selected levels (max 5) for each θ_s.

B.4.5 Sky radiance, $L_r(z,\theta,\beta)$ for $95° \leqslant \theta \leqslant 180°$ for selected levels (max 5) for each θ_s.

B.4.6 Sky plus terrain radiance $L_r(z,\theta,\beta)$ for $95° \leqslant \theta \leqslant 180°$ for selected levels (max 5) for each θ_s.

B.4.7 Contrast transmittance, $T_c(z,\theta,\beta)$ between object and sensor altitudes (max. 5 altitude intervals) for $0° \leqslant \theta \leqslant 85°$ and for each θ_s.

B.4.8 Contrast transmittance $T_c(z,\theta,\beta)$ between object and sensor altitudes (max. 5) for $95° \leqslant \theta \leqslant 180°$ and for each θ_s.

B.5 Additional Output From The Supplemental Eddington Computer Program

The standard Eddington computer program is employed as an integrated part of the model calculations of contrast transmittance. The following output from the program as modified by the delta-Eddington transformation of input parameters is available in tabular form for the base of each sub-layer and for each solar zenith angle:

- optical depths, τ and τ'
- components of Eddington diffuse radiance, $L_D(z)$ and $L_D{\cdot}(z)$
- total scalar irradiance
- downward diffuse irradiance
- upward diffuse irradiance
- solar irradiance
- total downward irradiance

APPENDIX C

SPECIFIC INPUT DATA FOR MODEL CALCULATIONS

Flight Number	C-401	C-466	C-469	C-469	REF-A	REF-B
Wavelength	550 nm	475 nm	475 nm	750 nm	550 nm	550 nm
Number of Layers	3	3	5	5	3	3
Tropopause Altitude	10 km	10 km	10 km	10 km	10 km	10 km
Upper Altitude Limit						
3rd Haze Layer			1.8 km	1.8 km		
2nd Haze Layer			1.5 km	1.5 km		
1st Haze Layer	1 km	1.3 km	1.2 km	1.2 km	3 km	1.3 km
Optical Scat. Ratio						
Stratosphere	1.2	1.2	1.2	1.8	1.3	1.3
Upper Trop.	1.2	1.2	1.2	1.8	1.3	1.3
3rd Haze Layer			7.3	20.8		
2nd Haze Layer			1.3	7.0		
1st Haze Layer	5.0	12.0	28.0	54.0	13.0	16.0
Single Scat. Albedo						
Stratosphere	.99	.99	.99	.99	.97	.97
Upper Trop.	.97	.97	.97	.97	.97	.97
3rd Haze Layer			.83	.83		
2nd Haze Layer			.97	.97		
1st Haze Layer	.97	.83	.83	.83	.97	.83
Surface Reflectance	.09	.07	.07	.33	.10	.07

APPENDIX D

GLOSSARY AND NOTATION

The notation used in reports and journal articles produced by the Visibility Laboratory staff follows, in general, the rules set forth in pages 499 and 500, Duntley *et al.* (1957). These rules are:

Each optical property is indicated by a basic (parent) symbol.

A presubscript may be used with the parent symbol as an identifier, *e.g.*, b indicates background while t denotes an object, *i.e.* target.

A postsubscript may be used to indicate the length of a path of sight, *e.g.*, r denotes an apparent property as measured at the end of a path of sight of length r, while o denotes an inherent property based on the hypothetical concept of a photometer located at zero distance from an object, *i.e.* target.

A postsuperscript* or postsubscript$_*$, is employed as a mnemonic symbol signifying that the radiometric quantity has been generated by the scattering of ambient light reaching the path from all directions.

The parenthetical attachments to the parent symbol denote altitude and direction. The letter z indicates altitude in general; z_t is used to specify the altitude of a target. The direction of a path of sight is specified by the zenith angle θ and the azimuth ϕ. In the case of irradiances, the downwelling irradiance is designated by d, the upwelling by u.

The radiometric symbols used herein now correspond to the OSA recommendations in Section 1 of the Handbook of Optics, McGraw-Hill Book Co., Driscoll and Vaughn (1978). Prior to June 1980, the symbol used for radiance I was n, for irradiance e was h, and for attenuation length was l.

Symbol	Units	
$A(z)$	none	Albedo at altitude z, defined $A(z) = E(z,u)/E(z,d)$.
$a(z)$	m^{-1}	Absorption coefficient
$C_o(z_t,\theta,\phi)$	none	Inherent contrast determined for a path of sight of zero length at the altitude of the object z_t in the direction of zenith angle θ and azimuth ϕ.
$C_r(z,\theta,\phi)$	none	Apparent contrast as determined at altitude z from the end of path of sight of length r in the direction of zenith angle θ and azimuth ϕ.
$D(z)$	none	Radiance distribution function $D(z) = \int_{4\pi} L(z,\theta',\phi')\sec\theta' d\Omega/a(z)$
$D(\lambda)$	none	Limb darkening factor relating the average sun radiance and the center sun radiance $D(\lambda) = {}_s\bar{L}_o/{}_sL_o$
E_λ	W/m^2	Spectral irradiance (formerly symbol H) defined as $E_\lambda = \int_{2\pi} L_\lambda(z,\theta,\phi)\cos\theta d\Omega$
E	$W/m^2\mu m$	broad band sensor irradiance, defined as $E = \int_0^\infty E_\lambda \overline{S_\lambda T_\lambda}\, d\lambda/\sigma\lambda$
$E(z,d)$	W/m^2	Irradiance produced by downwelling flux as determined on a horizontal flat plate at altitude z (formerly $h(z,d)$). In this report d is used in place of the minus sign in the notation $(H(z,-))$ which appears in Duntley (1969). This property may be defined by the equation $E(z,d) = \int_{2\pi} L(z,\theta',\phi')\cos\theta' d\Omega'$
$E(z,u)$	W/m^2	Irradiance produced by the upwelling flux as determined on a horizontal flat plane at altitude z (formerly $H(z,u)$). Here u is substituted for the plus sign formerly used in the notation $(H(z,+))$.
$g(z)$	none	Asymmetry factor $g(z) = \frac{1}{2}\int_{-1}^{1} P(z,\beta)\cos\beta d(\cos\beta)$
$H(z)$	m	Scale height at altitude z, the height of a homogeneous atmosphere having the density of the layer at altitude z.
L_λ	W/srm^2	Spectral radiance (former symbol N)
L	$W/srm^2\mu m$	Broad band sensor radiance is defined as $L = \int_0^\infty L_\lambda \overline{S_\lambda T_\lambda}\, d\lambda/\sigma\lambda.$
$L_o(z_t,\theta,\phi)$	W/srm^2	Inherent radiance based on the hypothetical concept of a photometer located at zero distance from an object at altitude z in the direction specified by zenith angle θ and azimuth ϕ.
$L_r(z,\theta,\phi)$	W/srm^2	Apparent radiance as determined at altitude z, from the end of a path of sight of length r at zenith angle θ and azimuth ϕ. This property may be defined by $L_r(z,\theta,\phi) = L_o(z_t,\theta,\phi)T_r(z,\theta) + L_r^*(z,\theta,\phi)$
$L(\lambda,T)$	W/srm^2	Black body radiance at wavelength λ and temperature T
$L_q(z,\theta,\phi)$	W/srm^2	Equilibrium radiance at altitude z with the direction of the path of sight specified by zenith angle θ and azimuth ϕ. This property is a point function of position and direction.
$L_*(z,\theta,\phi)$	W/srm^2	Path function at altitude z with the direction of the path of sight specified by zenith angle θ and azimuth ϕ. This property is defined by the equation $L^*(z,\theta,\phi) = \int_{4\pi} \sigma(z,\beta')L(z,\theta',\phi')d\Omega'$.

Symbol	Units	
$L_r^*(z,\theta,\phi)$	W/srm^2	Path radiance as determined at altitude z at the end of a path of sight of length r in the direction of zenith angle θ and azimuth ϕ.
$L_\infty^*(z,\theta,\phi)$	W/srm^2	Sky radiance at altitude z, zenith angle θ and azimuth ϕ. Also the path radiance for the path of sight of length ∞ from out of the atmosphere to altitude z.
${}_sL_\infty(z,\theta_s,\phi)$	W/srm^2	Apparent radiance of the center of the solar disk as determined from the end of a path of sight of length ∞ from out of the atmosphere to altitude z at the zenith angle of the sun θ_s.
$m_\infty(z,\theta)$	kg/m^2	Absolute air mass at angle θ $m_\infty(z,\theta)=\int_{z_t}^{\infty}\rho(z)dr$.
$m_\infty(z,\theta)/m_\infty(z,0)$	none	Relative optical air mass
$m(\theta_s)$	none	Relative optical airmass at zenith angle of the sun, shorthand for $m_\infty(z,\theta_s)/m_\infty(z,0)$.
$n(z)$	none	Refractive index
$P(z,\beta)$	sr^{-1}	Normalized phase function for single scattering. $P(z,\beta)=\sigma(z,\beta)/s(z)$
$Q(z)$	none	Optical scattering mixing ratio at altitude z. This quantity is defined as the ratio of the total volume scattering coefficient at altitude z, to the molecular (or Rayleigh) volume scattering coefficient at the same altitude z. $Q(z)=s(z)/{}_Rs(z)$
r	m	Path length, for paths of sight at zenith angles 0 to 70 degrees, $r=sec\theta\Delta z$
$s(z)$	m^{-1}	Total volume scattering coefficient as determined at altitude z. This property may be defined by the equations $s(z)=\int_{4\pi}\sigma(z,\beta)d\Omega={}_Rs(z)+{}_Ms(z)$ In the absence of atmospheric absorption, the total volume scattering coefficient is numerically equal to the attenuation coefficient.
${}_Ms(z)$	m^{-1}	Volume scattering coefficient for Mie *i.e.* aerosol, scattering at altitude z.
${}_Rs(z)$	m^{-1}	Volume scattering coefficient for Rayleigh *i.e.* molecular scattering at altitude z.
$T(z)$	$^\circ K$	Absolute temperature at altitude z.
$T_r(z,\theta)$	none	Radiance transmittance as determined at altitude z for a path of sight of length r at zenith angle θ (formerly referred to as "beam" transmittance). This property is independent of azimuth in atmospheres having horizontal uniformity. It is always the same for the designated path of sight or its reciprocal
$T_c(z,\theta,\phi)$		Contrast transmittance $T_c(z,\theta,\phi)=C_0(z_t,\theta,\phi)/C_r(z,\theta,\phi)$

Symbol	Units	
$T_\infty(z,\theta)$	none	Radiance transmitance for the path of sight at zenith angle θ from out of the atmosphere to the altitude z.
$\omega(z)$	none	Single scattering albedo $\omega(z)=s(z)/\alpha(z)$
z	m	Altitude, usually used as above ground level.
z_t	m	Altitude of any applicable target.
$\alpha(z)$	m^{-1}	Volume attenuation coefficient as determined at altitude z. $\alpha(z)=a(z)+s(z)$.
β	deg	Symbol for scattering angle of flux from a light source. It is equal to the angle between the line from the source to any unit scattering volume and the path of a ray scattered off this direct line.
Δ	none	Symbol to indicate incremental quantity and used with r and z to indicate small, discrete increments in path length r and altitude z.
$\epsilon(z)$	W/m^2	Scalar irradiance. This may be defined as the radiant flux arriving at a point, from all directions about that point, at altitude z (Tyler and Preisendorfer (1962)). $\epsilon(z)=\int_{4\pi}L(z,\theta',\phi')d\Omega'$.
${}_d\epsilon(z)$	W/m^2	Diffuse scalar irradiance ${}_d\epsilon(z)=\epsilon(z)-{}_s\epsilon(z)$.
${}_s\epsilon(z)$	W/m^2	Sun scalar irradiance at altitude z ${}_s\epsilon(z)={}_s\epsilon(\infty)T_\infty(z,\theta_s)$.
ζ	m	Radius of the earth.
θ	deg	Symbol for zenith angle. This symbol is usually used as one of two coordinates to specify the direction of a path of sight.
θ'	deg	Symbol for zenith angle usually used as one of two coordinates to specify the direction of a discrete portion of the sky.
θ_s	deg	Zenith angle of the sun.
λ	nm	Symbol for wavelength.
$\rho(z)$	kg/m^3	Density at altitude z.
$\sigma(z,\beta)$	$m^{-1}sr^{-1}$	Symbol for volume scattering function. Parenthetical symbols are z to designate altitude and β to designate the scattering angle from a source.
$\tau(z)$	none	Optical depth $\tau(z)=\int_z^{\infty}\alpha(z)dz$
ϕ	deg	Symbol for azimuth. The azimuth is the angle in the horizontal plane of the observer between a fixed point and the path of sight. The fixed point may be for example, true North, the bearing of the sun, or the bearing of the moon. This symbol is usually used as one of two coordinates to specify the direction of a path of sight.